

GEOSTATISTICAL ANALYSIS OF LAND USE/LAND COVER CHANGES
AND POPULATION GROWTH TRENDS IN THE
KOMADUGU-YOBE RIVER BASIN IN NIGERIA

A THESIS IN
Environmental and Urban Geosciences

Presented to the Faculty of the University
of Missouri-Kansas City in partial fulfillment of
the requirements for the degree

MASTER OF SCIENCE

By
INGRID MILENA TOBAR

B.S., Environmental Studies
University of Missouri-Kansas City, 2008

Kansas City, Missouri
2012

© 2012

INGRID MILENA TOBAR

ALL RIGHTS RESERVED

GEOSTATISTICAL ANALYSIS OF LAND USE/LAND COVER CHANGES
AND POPULATION GROWTH TRENDS IN THE
KOMADUGU-YOBE RIVER BASIN IN NIGERIA

Ingrid Milena Tobar, Candidate for the Master of Science Degree

University of Missouri-Kansas City, 2012

ABSTRACT

The Komadugu-Yobe River located in northeastern Nigeria is an important tributary of Lake Chad. Since the 1970s, the Komadugu-Yobe basin has experienced significant changes in population density and land use/land cover. The present study consists of the application of geostatistical methods to examine the land use/land cover and population density dynamics in the river basin area bound between 11° and 13° N latitude and between 8° and 14° E longitude, covering approximately 151,060.95 Square Kilometers. The geostatistical methods applied include kriging interpolation, spatial autocorrelation, overlapping neighborhood statistics with Pearson's correlation coefficient, indicator variogram, rose diagram, and histogram analysis. Spatiotemporal changes for the two variables were analyzed for five years of observation: 1970, 1986, 2000, 2005, and 2009.

The time-series summary and kriging interpolation of yearly precipitation identified the year 1980 as a time period of significance for the present study. The calculation of net changes in land use/land cover indicate significant variation in rainfed cropland, mosaic

cropland, mosaic vegetation, grassland, sparse vegetation, and vegetation regularly flooded. Spatial autocorrelation analysis showed that the distribution of these classes is clustered.

A new geostatistical tool was designed to calculate the overlapping neighborhood statistics with Pearson's correlation coefficient between the land use/land cover and population density datasets. Output maps show areas of direct correlation in red, inverse correlation in blue, and no relation in pale yellow. The 10x10 neighborhood cell unit showed a clearer correlation between the variables in certain zones of the study area.

The ranges calculated from variogram plots of land use/land cover and population density were used to build rose diagrams. These diagrams depict the classes most closely related to population density: mosaic cropland, rainfed cropland, sparse vegetation, mosaic vegetation, and grassland. Population density histograms show a nearly normal distribution, which produced similar range and direction values for all the years of observation. This indicates that when variable changes are anisotropic and linear in time the ranges of the variogram functions are similar. The variogram function is a useful spatial comparison tool to inspect a single period of observation, but the analysis of trends over time may require a different methodology.

APPROVAL PAGE

The faculty listed below, appointed by the Dean of the College of Arts and Sciences have examined a thesis titled “Geostatistical Analysis of Land Use/Land Cover Changes and Population Growth Trends in the Komadugu-Yobe River Basin in Nigeria” presented by Ingrid Milena Tobar, candidate for the Master of Science degree, and certify that in their opinion it is worthy of acceptance.

Supervisory Committee

Jejung Lee, Ph.D., Committee Chair
Department of Geosciences

James B. Murowchick, Ph.D.
Department of Geosciences

Wei Ji, Ph.D.
Department of Geosciences

CONTENTS

ABSTRACT	iii
ILLUSTRATIONS	viii
TABLES	x
ACKNOWLEDGEMENTS	xi
Chapter	
1. INTRODUCTION	1
1.1 Site Location	2
1.2 Definition of the Study Area	3
1.3 Objective	3
2. LITERATURE REVIEW	5
2.1 Water Level Reduction at Lake Chad	5
2.2 Hydrology of Lake Chad	6
2.3 Climate and Precipitation	8
2.4 Human-induced Pressure on the Water Budget	9
2.5 Land Use/Land Cover Change	11
2.6 Population and Land Use/Land Cover Dynamics	16
2.7 Geostatistical Methods in Land Use/Land Cover Change Detection	18
2.8 Relevance of the Study	20
3. DATA SOURCES AND PRE-PROCESSING	22
3.1 Historical Climate and Precipitation Data	22
3.1.1 Data Assembly into a Database	24
3.2 Satellite Imagery	25
3.2.1 Satellite Image Classification Process	28

3.3	Pre-classified Land Use/Land Cover Data.....	29
3.4	Standardization of Land Use/Land Cover Classes.....	30
3.5	Population Density.....	31
3.5.1	Cell Size Limitations.....	35
4.	GEOSTATISTICAL ANALYSIS METHODOLOGY	36
4.1	Kriging Interpolation	36
4.2	Spatial Autocorrelation	37
4.3	Overlapping Neighborhood Statistics with Correlation Coefficient.....	38
4.4	Variogram Plots and Rose Diagram Analysis	40
5.	RESULTS AND DISCUSSION	46
5.1	Precipitation Data.....	46
5.1.1	Time-Series Summary	46
5.1.2	Kriging Interpolation	46
5.2	Land Use/Land Cover	49
5.2.1	Percent Net Change.....	51
5.2.2	Spatial Autocorrelation	52
5.3	Population Density and Land Use/Land Cover	53
5.3.1	Overlapping Neighborhood Statistics with Correlation Coefficient.....	54
5.3.2	Variogram Plots and Rose Diagram Analysis	60
5.3.3	Population Density Histogram Analysis.....	62
6.	CONCLUSION.....	70
	REFERENCES	73
	VITA.....	76

ILLUSTRATIONS

Figure	Page
1.1. The Sahel and Approximate Location of Lake Chad.....	2
1.2. Study Area.	4
2.1. USGS Earthshot Historical Images of Lake Chad.....	5
2.2. Komadugu-Yobe River System.....	6
3.1. Weather Stations Near the Study Area.....	25
3.2. Landsat Thematic Mapper (TM) Satellite Imagery for 1986.....	26
3.3. Landsat ETM+ Pan Mosaic Satellite Imagery for 1999-2003.....	27
3.4. Population Density.....	33
4.1. Spatial Autocorrelation Distribution and Significance Levels.	37
4.2. Overlapping Neighborhood Statistics Toolbox Modules.	39
4.3. General Shape of the Semivariogram Function.	40
4.4. Sample Indicator Map for Mosaic Cropland Class Converted to Binary.	43
4.5. Example Variogram Plots for the 1970 Rainfed Cropland Class.	45
5.1. Yearly Precipitation Records for Weather Stations Near the Study Area.	47
5.2. Decadal Average Precipitation Distribution in the Study Area.	48
5.3. Land Use/Land Cover Classified Raster Images.	50
5.4. Land Use/Land Cover Percent Net Change.	52
5.5. Correlation Coefficients for 3x3-Cell Overlapping Neighborhood.	56
5.6. Correlation Coefficients for 5x5-Cell Overlapping Neighborhood.	57
5.7. Correlation Coefficients for 7x7-Cell Overlapping Neighborhood.	58
5.9. Side-by-side Comparison of Land Use/Land Cover and Correlation Coefficients.	60

5.10. 1970 Land Use/Land Cover and Population Density Rose Diagrams.....	63
5.11. 1986 Land Use/Land Cover and Population Density Rose Diagrams.....	64
5.12. 2000 Land Use/Land Cover and Population Density Rose Diagrams.....	65
5.13. 2005 Land Use/Land Cover and Population Density Rose Diagrams.....	66
5.14. 2009 Land Use/Land Cover and Population Density Rose Diagrams.....	67
5.15. Log-Transformed Population Density Histograms.....	69
6.1. Similar Rose Diagrams between Land Use/Land Cover and Population Density.....	71

TABLES

Table	Page
3.1. Stations with Historical Climate Data Available.....	23
3.2. Precipitation Data Source by Station.....	24
3.3. Land Use/Land Cover Data Source Summary.....	30
3.4. Land Use/Land Cover Reclassification Scheme.....	32
5.1. Land Use/Land Cover Area Summary by Class and Year.....	49
5.2. Land Use/Land Cover Percent Net Change.....	51
5.3. Spatial Autocorrelation Metrics.....	53
5.4. Pearson’s Correlation Results from Overlapping Neighborhood Statistics Tool.....	54
5.5. Indicator Variogram Range Values.....	61
5.6. Population Density Sample Statistics and Log-Transformed Values.....	68

ACKNOWLEDGEMENTS

Foremost, I would like to express my sincere gratitude to my advisor Dr. Jejung Lee for his continuous support of my research, for his patience despite the geographical challenges we encountered in this venture and for his enthusiasm and dedication to our Hydro Lab. His time and efforts have been pivotal in the development of this thesis.

I remain indebted to Professors James Murowchick and Wei Ji for serving in my Supervisory Committee and for encouraging me throughout my undergraduate and graduate studies at University of Missouri, Kansas City. I also wish to give special thanks to Professor Daniel Hopkins for teaching me to approach technical writing in a creative manner and for instilling in me curiosity for the history and philosophy of cartography.

I would also like to extend my sincere thanks to Rakiya Baba-maaji for her assistance on data collection, classification, and patient guidance with questions and last minute requests. Thank you for being an exemplary research partner, a knowledgeable mentor, and a true friend.

Last but not the least; I would like to thank my two ‘favorite people’, who inspire me to strive for excellence in my academic endeavors and to set high standards for myself in all aspects of life. I dedicate this work to my parents Luis Tobar and Mercedes Bernal de Tobar. Thank you for your love, continued support, and for patiently understanding my schedule limitations during the course my research.

CHAPTER 1

INTRODUCTION

Located in the southern fringe of the Sahel, the transition zone between the Sahara desert and the African savannas, Lake Chad constitutes an essential water resource for its four neighboring countries: Niger, Nigeria, Chad and Cameroon. This lake has undergone drastic water level fluctuations in the last few decades. Severe droughts in the periods between 1968-1974 and 1983-1985 (Isiorho and Njock-Libii, 1996) and deficient rainfall regimes since the 1960s (Kimmage and Adams, 1992) have contributed to its depletion, reducing its surface area to less than one tenth of its size (Grove, 1996; Obinna, 2011). Fishermen and farmers of the region have suffered the consequences of this change, having to adapt their sustenance activities to a reduced water budget or migrate to other areas. Although climate change has been identified as a decisive factor in the water level reduction of Lake Chad (Coe and Foley, 2001), anthropogenic factors that contribute to water balance fluctuations also require thorough examination.

Understanding the relationship between population growth and land use/land cover changes, taking into account historical precipitation trends in the study area, could help illustrate the dynamics of water level fluctuations at Lake Chad. In order to conduct this analysis, the present study summarizes four decades of precipitation records, land use/land cover change maps, and population density data for a section of the area drained by the Komadugu-Yobe river system that feeds into Lake Chad from the northwest. Multiple geostatistical methods are applied, including kriging interpolation, spatial autocorrelation, overlapping neighborhood statistics with Pearson's correlation coefficient, indicator variogram, rose diagram, and histogram analysis, in order to quantify and illustrate

spatiotemporal changes in precipitation, land use/land cover, and population, observed in the years 1970, 1986, 2000, 2005, and 2009 in the study area.

1.1 Site Location

The Sahel is a transition zone that stretches longitudinally across the African continent, separating the Sahara desert on the north and the savannas on the south (Figure 1.1). Lake Chad is located in the heart of the Sahel, at the boundary junction of Niger, Nigeria, Chad and Cameroon; however, most of the lake resides in the country of Chad. Although the Sahel is a semiarid area, agricultural production is the foundation of the region's economy. However, despite its relatively high productivity, the basin of Lake Chad lies in a very sensitive environmental fringe that is not only prone to droughts, but also has been identified as one of the poorest regions of the world (Obinna, 2011). The future of the communities that rely on Lake Chad for sustenance is uncertain, as the lake has been experiencing a progressive desiccation trend for the last five decades.

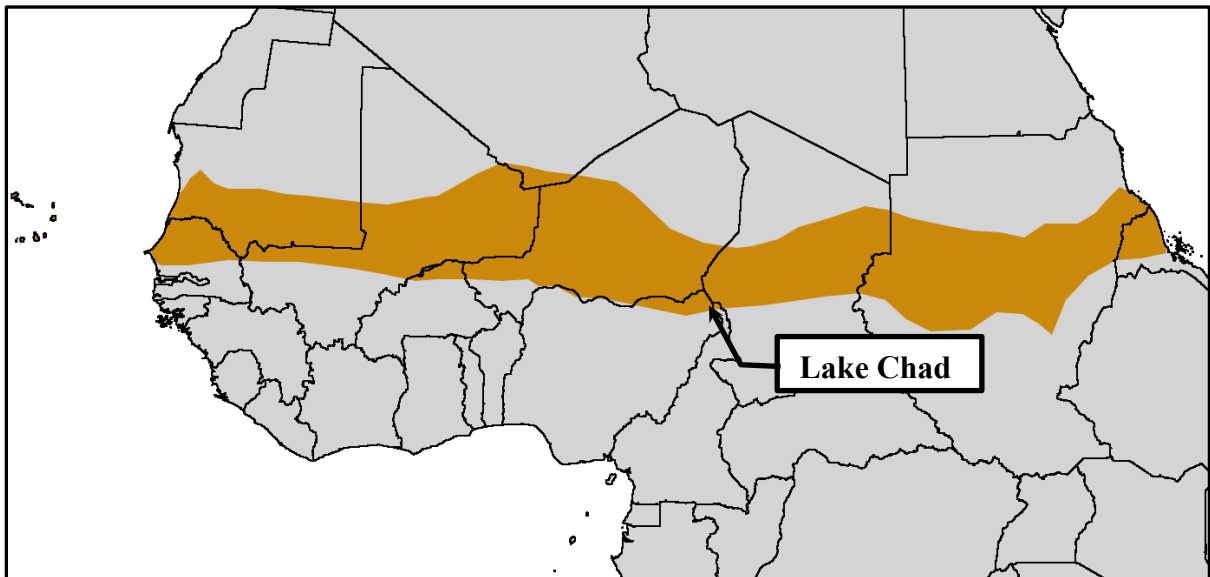


Figure 1.1. The Sahel and Approximate Location of Lake Chad. (Courtesy: Koenig, Felix.

“A map of Africa: the Sahel highlighted in orange.” 2011)

Lake Chad's moderate depth is one of the factors that make it highly sensitive to droughts and prone to desiccation. The lake is relatively shallow, with a maximum depth of approximately 7 m (Coe and Foley, 2001). In addition, the combined effects of low humidity, variable precipitation, and the predominantly high temperatures typical of the Sahel also influence the lake's reduction rate. It is estimated that at least 80% of Lake Chad's water is lost through evaporation alone (Roche, 1973). In addition, demand for water resources in the basin is projected to increase, which may significantly accelerate the current shrinkage rate of Lake Chad.

1.2 Definition of the Study Area

In order to narrow the scope of the present study, a study area was delineated (Figure 1.2) that included the Komadugu-Yobe River drainage system, located in northeastern Nigeria. The final study area is bound between 11° and 13° N latitude and between 8° and 14° E longitude and it covers approximately 151,060.95 Square Kilometers.

1.3 Objective

The main goal of the present study is to conduct a geostatistical analysis of the land use/land cover changes and population growth trends observed between 1970 and 2009 in the immediate area of the Komadugu-Yobe River system in Nigeria. The purpose of this analysis is to determine whether the land use/land cover changes observed during this time period may be correlated to the population density changes in the area.

In an effort to quantify the relationships observed between land use/land cover change and population density, various geostatistical tools were applied, including spatial autocorrelation, overlapping neighborhood statistics with Pearson's correlation coefficient, indicator variogram, rose diagram and histogram analysis. In addition, precipitation data was

analyzed using a kriging interpolation technique to assist in the identification of periods of significant changes in precipitation distribution throughout the study area.

It is the objective of the present study to provide a basic framework in geostatistical analysis of land use/land cover and the potential correlation of this variable with population density, with the ultimate goal of supporting the development of an integrated overview of the anthropogenic factors that influence the hydrologic regime of Lake Chad.

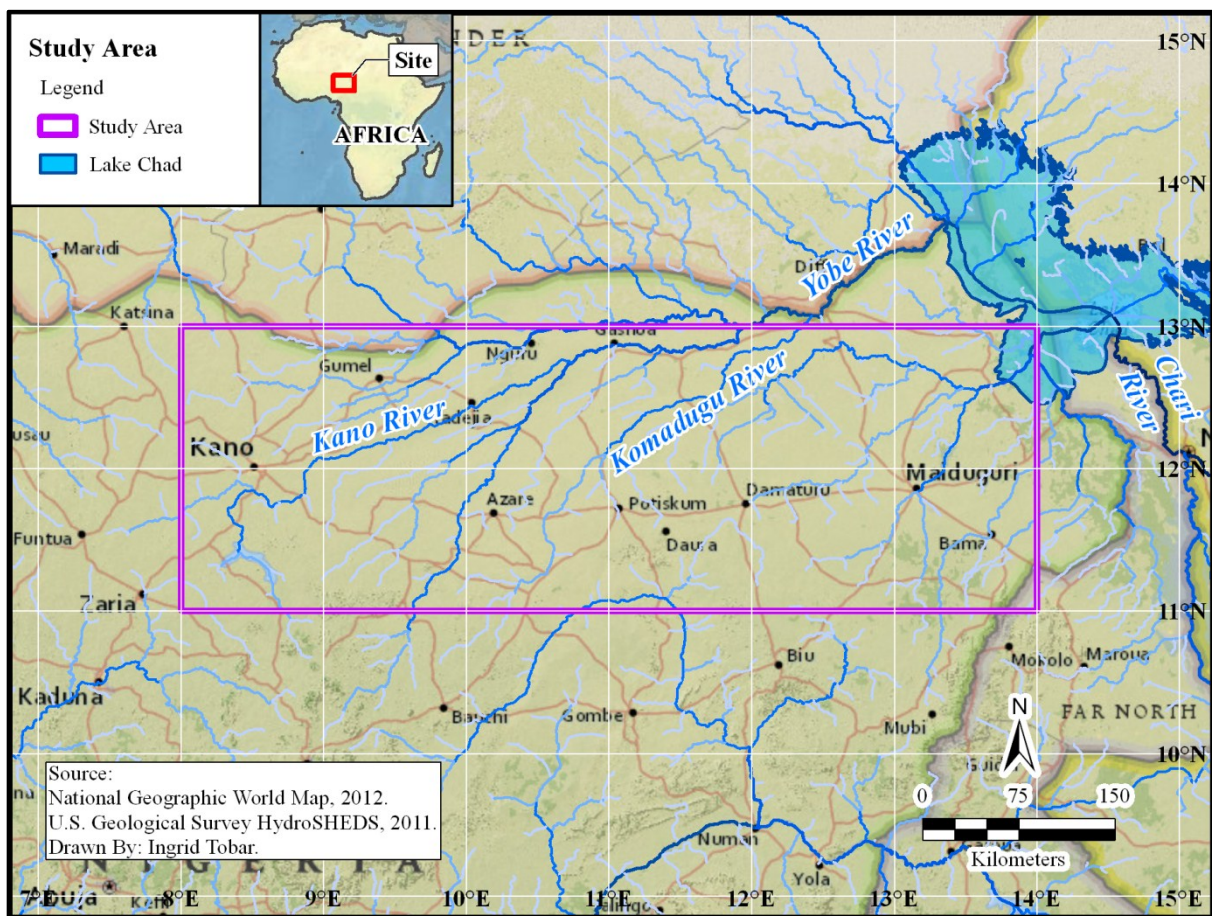


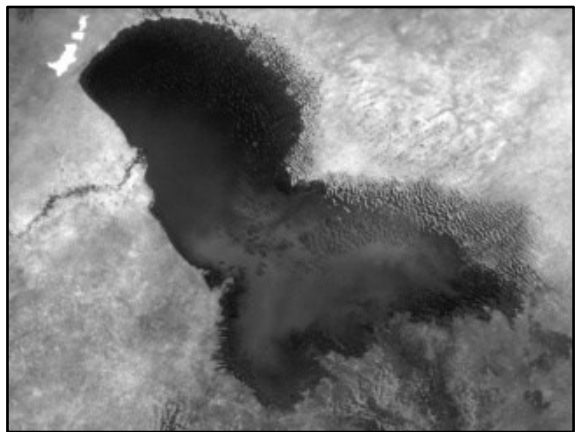
Figure 1.2. Study Area.

CHAPTER 2

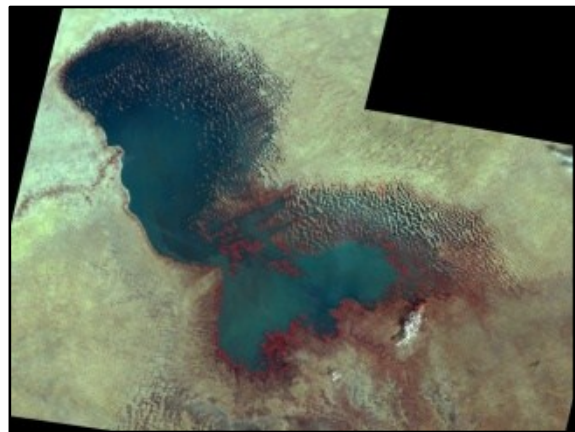
LITERATURE REVIEW

2.1 Water Level Reduction at Lake Chad

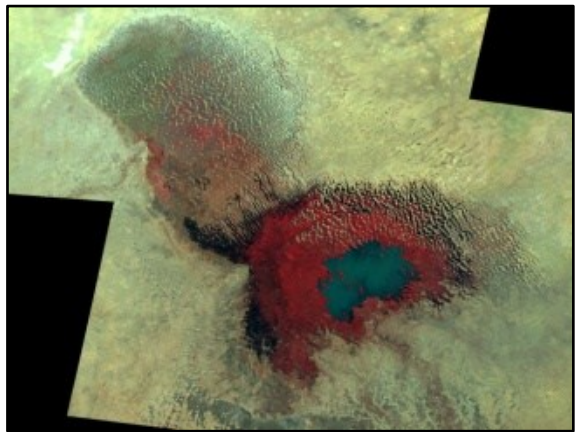
The water level at Lake Chad has diminished progressively over the last 50 years. The lake's area has been reduced from 25,000 km² in 1963 to 10,000 km² in 1973 (Coe and Foley, 2001). Satellite imagery confirms that the lake's current extent is now only about a twentieth of its original size (Figure 2.1). The former open water surface of the lake is now characterized by islands and small interconnected ponds. As the lake dries up, the previously fertile lands surrounding it become dry and unproductive.



1963 – Argon Satellite



1973 – Landsat 1 MSS



1987 – Landsat 5 MSS



2007 – Landsat 5 MSS

Figure 2.1. USGS Earthshot Historical Images of Lake Chad. (USGS, 2010)

2.2 Hydrology of Lake Chad

The Chari River is Lake Chad's largest tributary, transporting about 90% of the runoff of the basin (FEWS, 1997). The Chari River runs north-northwest from the southern boundary of Chad, and passes through the city of N'Djamena before entering Lake Chad. Despite the significance of the Chari River in the hydrology of Lake Chad, the present study focuses on the Komadugu-Yobe River system that feeds into the lake from the west-southwest (Figure 2.2). Although the flow of the Komadugu-Yobe accounts for only about 10% of the runoff for the entire basin, it still constitutes an important source of recharge for Lake Chad.

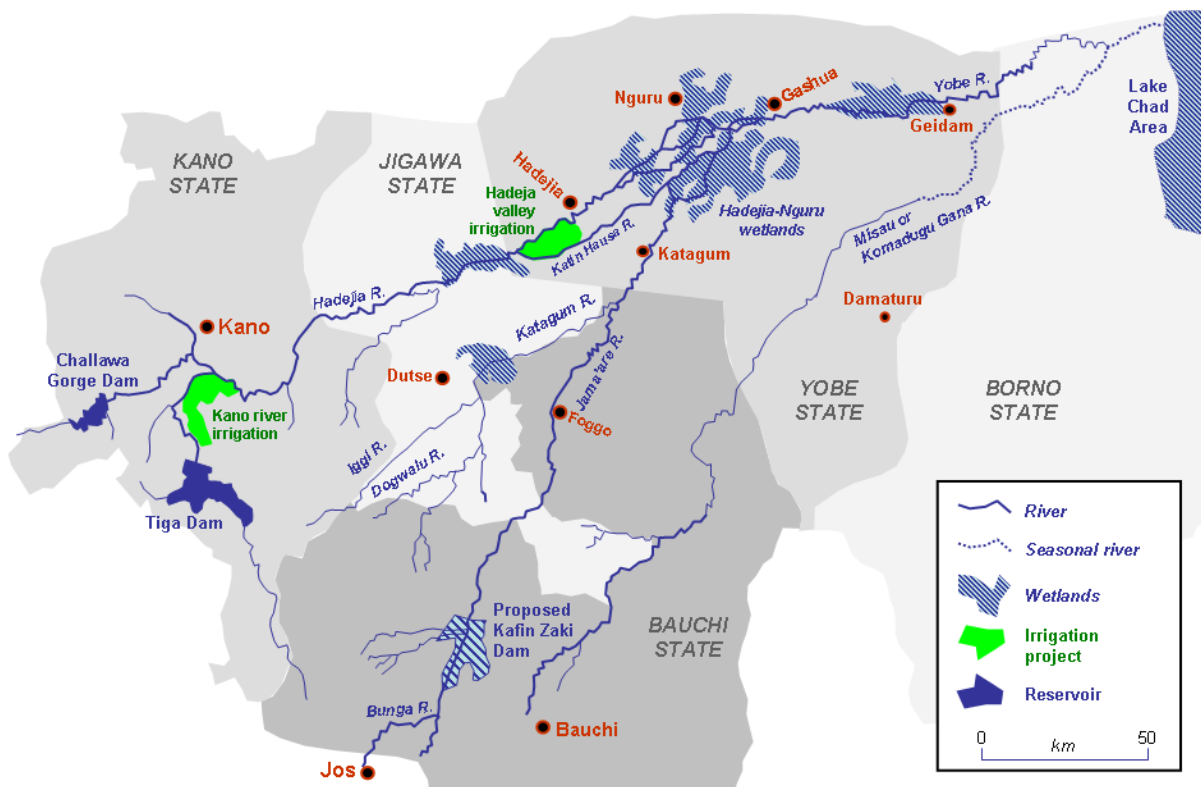


Figure 2.2. Komadugu-Yobe River System. (Courtesy: Aymatth2. "Sketch map of the catchment area of the Yobe river in north-east Nigeria." 2009)

The Komadugu-Yobe River system lies in the northeastern part of Nigeria. The catchment of the Yobe River is located near the city of Kano (where its upstream reach is known as Kano River) and the river flows east-northeast, encompassing the Hadejia-Nguru wetlands (between the cities of Hadejia and Nguru), ending at Lake Chad near the city of Bisagana, Nigeria. The Komadugu River flows north-northeast from Bauchi state, Nigeria, and its confluence with the Yobe River is located near the city of Maine Soroa, Niger. This drainage system, and its wetland network, plays an important role in the overall water balance scheme of Lake Chad.

The Komadugu-Yobe River undergoes seasonal flow fluctuations that sustain a network of wetlands and pools along its floodplain. A study of recharge trends in a small area of the Sahel demonstrated that recharge of the underlying aquifers depends largely on water infiltration from pools that emerge during flood events and persist throughout drought periods (Desconnets et al. 1997). This study found that that after flood events, aquifer levels tend to rise more rapidly at the immediate vicinity of the pools than at areas distant from them, demonstrating their importance in aquifer recharge dynamics. This stresses the importance of the Komadugu-Yobe River's pools and wetlands in the balance of aquifer levels at the western fringe of the basin of Lake Chad.

However, it is clear that the stability of Lake Chad's water budget does not depend on aquifer recharge alone and other factors must be taken into consideration. Since the 1960s, Sahelian water-table levels have experienced a long-term rise despite the negative impact of droughts, reaching the highest levels ever recorded (Leduc, Favreau, and Schroeter, 2001). Despite this fact, Lake Chad's surface area has shown a continuously declining trend,

demonstrating that in addition to groundwater levels, climate and precipitation, land use/land cover, and human induced stresses to the water budget also require further examination.

2.3 Climate and Precipitation

The predominant climate of the Komadugu-Yobe River area is semi-arid, and the precipitation regime depends on the seasonal migration of the Inter-Tropical Convergence Zone (ITCZ) (Thompson and Polet, 2000). The spatial distribution of precipitation in the Sahel marks the difference between productive areas and desertification-prone landscapes. Rain probability in the Sahel shows strong anisotropy because it depends on the West African monsoon, defining a stronger rainfall probability in the southern areas of the Sahel (Cappelaere et al., 2009). In addition, the intensity and distribution of rainfall in the Sahel region is the major control of runoff (Desconnets et al., 1997), which directly impacts water flow towards the lake. These facts highlight the importance of studying the spatial distribution of rain probability and flow direction in the study area.

The Sahelian region endures extreme climatic variability between severe drought and excessive flooding (Grove, 1996). However, in comparison with other sub-Saharan African locales, the droughts of the Sahel have been less pronounced. For example, drought indexes in the Sahel are not as intense as those observed in Somalia because the region receives just enough precipitation to maintain somewhat stable conditions (Obinna, 2011). This is probably due to Lake Chad's proximity to the area of influence of the West African monsoon. Under different climatic conditions, the rate of reduction of Lake Chad's surface area may accelerate, having a devastating impact on the human populations that depend on it.

Although the climate of Lake Chad's western basin is less harsh than that of the eastern Sahel, the area still endures extreme climatic variations. The hydrology of Lake Chad is

affected by annual precipitation variability and it has been impacted by two marked droughts that took place in the periods 1972 – 1978 and 1980 – 1987 (Kimmage and Adams, 1992). Overall, in the last three decades, a 25% reduction in precipitation has been observed in micro-scale study areas near the city of Niamey, Niger, located west of the basin of Lake Chad (Boulain et al., 2006). Similar precipitation reduction patterns are observed at certain weather stations in the study area, however, in order to fully understand and interpret the changes in precipitation in the basin of Lake Chad, a detailed inventory of historical precipitation records must be constructed, and the factors that influence precipitation variability in this region must be analyzed further.

The droughts of the Sahel represent an important time period in the water balance cycle of the region, but they may need to be examined in the context of a larger scheme. Most studies describe Sahelian precipitation trends as a relatively stable regime with two marked droughts, however, in the long run the observed changes may actually depict a progressively declining trend up to the year of 1983 (approximately) and a linear increasing trend thereafter (Boulain et al., 2009). This implies that time elapsed should be an important factor of consideration in the study of water balance dynamics in the region.

2.4 Human-induced Pressure on the Water Budget

The population of the Sahel doubles every 20 years, and various studies have demonstrated that changes in vegetation are closely related to human population, access to technology, market needs and socio-economic policies (Taylor et al., 2002). Lake Chad provides sustenance to nearly 30 million inhabitants (Obinna, 2011). People in this region depend on Lake Chad and its tributaries for fishing, farming and agricultural activities. Slight changes in the water budget of the basin can greatly impact the populations that depend on it.

The Komadugu-Yobe floodplain is important for the economy and livelihood of locals due to its high yield in rice and vegetables (Kimmage and Adams, 1992). In addition to the production of millet, sorghum, rice, wheat and vegetables, the wetlands sustain fishing and livestock rearing practices. These activities depend on rain variability and flood cycles, yet they provide the livelihood of nearly 1.2 million people in the Hadejia-Nguru wetlands alone (Thompson and Polet, 2000). Historically, agriculture has been the main economic activity in the basin of Lake Chad, and it is driven by population growth and increased demand for food availability.

Population growth can cause a direct environmental impact on the water budget of Lake Chad. Since the 1940s the Sahel has experienced a population increase at a yearly rate of 3%, which is associated with the extension of cultivated land (Seguis et al., 2004). Thompson and Polet (2000) observed that the discharge of the Hadejia River decreases rapidly along the Hadejia-Nguru wetlands due to the natural inundation of flatlands used for rice cultivation. The flooding of the flatlands used for cultivation and filling of natural pools in the floodplain not only alters the natural landscape, but also, reduces the flow downstream to Lake Chad impacting the basin's water budget.

An important consideration must be made in studying the water balance of the watershed: the environmental pressures upstream of the lake can have pronounced impact downstream, at the lake itself. In a study of the spatial and temporal variability of drought indices, Obinna (2011) concludes that water abstraction for irrigation and pasturing upstream of Lake Chad exacerbates the desiccation of intermittent streams during drought periods, which results in reduced flow at the lake. Similarly, in a study on wetland agricultural productivity in the Hadejia River, Kimmage and Adams (1992) assert that the economic value of wetland

production extends beyond their immediate geographical area to include downstream regions. This illustrates the importance of identifying the spatial distribution of environmental pressures on the water cycle throughout the watershed.

In conjunction, the development of the Kano River Irrigation Project (KRIP) and the construction of the Tiga and Challawa Gorge dams have also modified the natural runoff patterns of the Hadejia River system (Thompson and Polet, 2000). These developments have altered the flow of the water, and the timing and peak of flood flows in the basin (Kimmage and Adams, 1992). These developments, along with the impacts of the droughts of the 1970s and 1980s have triggered the environmental degradation of the floodplains (Kimmage and Adams, 1992). However, a detailed impact assessment of these developments is necessary in order to determine the proportion of impact attributable to each of these developments.

Although the human water consumption in the basin has increased in response to the population growth, this variable alone cannot explain the reduction in the surface area of Lake Chad. Between 1953 and 1979, only about 20% of the reduction in the surface area of Lake Chad may be attributed to the human water use (Coe and Foley, 2001; Vuillaume, 1981; Olivry, 1996). Climate variability, characterized by decreasing precipitation trends, and intensified human water consumption through irrigated agriculture are mutually responsible for the observed shrinkage of Lake Chad after 1975 (Coe and Foley, 2001; Birkett, 2000). The interactions between these variables and their individual effects on the basin's water budget require further examination.

2.5 Land Use/Land Cover Change

Land use/land cover changes can occur naturally in the landscape as successional processes; however, often landscapes are modified by humans in response to a specific need

for the population that depends on the land in question. For example, in the Sahel, agriculture and wood harvesting for cooking fuel are the major activities that cause modifications of the land cover (Cappelaere et al., 2009). Land use/land cover change from forest to agriculture is a common process that affects the availability of natural resources, biodiversity conservation, and water cycles. Although the land use/land cover classification process is rather subjective and it is difficult to identify a single ideal classification system (Anderson et al., 1976), analysis of these changes is important in the adequate management of natural resources and the sustainable development of populations.

According to Anderson et al. (1976), the minimum land use/land cover map unit is based on the scale and resolution of the original remote sensor used to acquire the aerial photograph or satellite image, but it also depends on the scale of data compilation, and ultimately on the scale of the final classified coverage. These guidelines were followed in the present study in order to identify the minimum effective cell size for the creation of a land use/land cover classification of the study area from available satellite imagery.

Land use/land cover changes can be analyzed by pre-classification and post classification methods. Pre-classification methods apply image analysis algorithms to highlight change vs. no-change areas, whereas post classification methods compare land use/land cover classes derived from images to indicate changes from one class to another between two different time periods (Mubea, Mundia, and Kuria, 2011). Due to the ease of application and reproducibility of results, a post classification method was applied in the present study to identify the land use/land cover transitions in the study area.

Historical aerial photographs and satellite images of the basin of Lake Chad show that since the 1950s agricultural expansion and land clearing associated with population growth

describe the predominant land use/land cover theme. Runoff has increased due to land clearing and the wooded savannah land cover of the Sahel has been replaced by millet fields and fallows (Leduc, Favreau, and Schroeter, 2001). Intensive flood rice farming is now practiced throughout the wetlands of Lake Chad. Thompson and Polet (2000) indicates that flood rice farming is the land use most dependent on the hydrologic regime of the basin and its distribution has increased in response to the increased food demand for the growing population of the Sahel.

Land use/land cover change proportion and location are equally important in the examination of the overall transition of an area of study (Boulain et al., 2009). Detailed examination of the spatial distribution of land use/land cover changes is facilitated through the use and availability of satellite imagery and geographic information systems (GIS). Aerial photography and satellite imagery can be used to complement ground surveys in order to produce an accurate inventory of land use/land cover changes in a particular study area (Anderson et al., 1976). These tools can be used to extract information for a study area, compare geospatial datasets, and perform statistical analysis.

A standardized land use/land cover classification system is necessary in order to examine the value of environmentally important areas such as floodplains, wetlands, and to assist in the effective planning of residential and industrial development land uses (Anderson et al., 1976). However, in addition to standardization of the classification methodology, analysts should pay special attention to the accuracy of the classified end product. The accuracy of land use/land cover change detection depends on the precision of the classification and it may be subject to error propagation (Mubea, Mundia, and Kuria, 2011). For example, misrepresentation in land use/land cover classes, deficient sampling points, and subjective

variation may alter the results of an initial classification that may be used as a base dataset for further analysis. Since land use/land cover classifications are generally designed to meet the needs of a particular user, general criteria guidelines should be adopted in order to develop a framework that meets the needs of the majority of users (Anderson et al., 1976). In the case of satellite image classification for the Lake Chad basin, I adopted the Anderson classification system, modified according to the extent and distribution of land use/land cover changes observed in the study area.

Since 1950 a large proportion of the land cover of the Sahel region evolved from savanna to agricultural land use (Seguis et al., 2004). However, the most significant land use/land cover transformations seem to take place after 1975, particularly the dramatic increase in area extent of croplands (Boulain et al., 2006). An overall increase in runoff and erosion rates in the catchment of Lake Chad has been observed in conjunction with a decrease in vegetation cover, land clearing, and cropland emergence (Boulain et al., 2009; Seguis et al., 2004). Land clearing decreases the content of organic matter in the top soil, enhancing surface crusting, which leads to increased runoff (Leduc, Favreau, and Schroeter, 2001). These changes are related to the demographic expansion of the region and the heightened demand for agricultural production.

In a study conducted at a small Sahelian catchment located west of the study area, Seguis et al. (2004) observed an increase of cropland area from 6 to 17% between 1950 and 1975, and from 17 to 56% between 1975 and 1992. The researchers also calculated an eroded surface area increase from 7 to 21% between 1950 and 1975, which caused a doubling in the annual runoff rate. Although increased runoff is associated with population growth and land use/land cover changes, Seguis et al. (2004) makes emphasis on the fact that the geographic

distribution of land use/land cover changes cannot be considered the sole determining factor in the increased runoff observed. In fact, other contributing factors must be at play and their impact on the hydrology of Lake Chad must also be considered.

In fact, several environmental factors can interact dynamically to contribute to the balance of the region's water budget and they cannot be measured independently. A study of the precipitation trend in the Sahelian region finds 20% decrease in precipitation in recent decades associated with land use/land cover change; however, the observed land use/land cover changes are not significant enough to explain this overall declining precipitation trend (Taylor et al., 2002). This illustrates the fact that examination of the water budget of Lake Chad requires a multivariable approach and individual variable impacts may not always be isolated from the greater impact scheme.

The increase of the water-table level in Lake Chad is an unusual observation that requires further examination and underscores the importance of quantifying the effects of land use/land cover change in the basin of Lake Chad. In recent decades, land clearing had greater influence on the Sahelian water-table than climatic variation, to the point that this type of land use/land cover change may actually hide the negative impacts of the droughts of the 1970s and 1980s on the water-table (Leduc, Favreau, and Schroeter, 2001). The impact of land use/land cover change on the water balance of the Sahel is larger than that observed from the long-term drought regime (Cappelaere et al., 2009). Various studies of the General Circulation Model's (GCM) sensitivity to vegetation cover show a negative correlation between rainfall and vegetation degradation (Taylor et al., 2002). These observations should serve as an indication of the importance of land use/land cover change in the hydrology of Lake Chad; yet, they should not be used to arrive at the conclusion that land use/land cover

change effects can be measured and quantified in isolation from other relevant factors such as climate change or precipitation variability.

2.6 Population and Land Use/Land Cover Dynamics

Meyer and Turner (1992) explain that “human impact [on the environment] is a product of the number of people, the level at which they consume, and the character of material and energy flows in production and consumption”. This basic notion underscores the role of population growth in landscape transformation over time. In some areas of Africa, population growth between 1950 and 1995 has increased nearly twentyfold (Seguis et al., 2004). An increase in population of this magnitude presupposes a dramatic change in allocation and use of natural resources; therefore, changes in land use/land cover towards the classes that provide for the sustenance of larger human populations are expected. The land use/land cover distribution is not only influenced by spatial continuity factors, but also determined by a set of sociocultural factors (Judex, Thamm, and Menz, 2006). Thus, the examination of land use/land cover change can be complemented by the analysis of population density trends.

However, measuring the impact of population growth on land use/land cover change is not always achievable in all settings. At a global macro-scale, population density and natural resource demand, reflected on land use/land cover changes, are directly related; however, at increasingly smaller scales, other variables must be taken into consideration to account for spatial variation in land use/land cover (Meyer and Turner, 1992). For example, a study of land use dynamics and demographic change in southern Burkina Faso shows a strong correlation between population and land use at all spatial levels, however, at regional levels, only correlations between cropland and forest land covers were perceptible (Ouedarogo,

2010). This is an important consideration that was taken into account in the present study for the determination of the study area, because the effect population density on land use/land cover may be imperceptible at smaller scales.

Agriculture is the most closely related land use/land cover class to population density, since observations demonstrate that under sustained population growth agricultural use increases, and under declining population rates agricultural use decreases (Meyer and Turner, 1992). In a study of land use/land cover changes in a West African catchment, Judex, Thamm, and Menz (2006) found a positive correlation between population density and areas of the coverage classified as settlements or as agricultural land use. This is a clear indication that population density and agricultural land use/land cover change in the Sahel display a close positive relationship.

Furthermore, projected land use models indicate that a reduction in vegetation cover will be prevalent in the future Sahelian landscape, as population density continues to grow rapidly (Taylor et al., 2002). The rate of land use/land cover change from modeled projections cannot be determined with accuracy. However, a good indication of the expected outcome may be deducted from the patterns observed in recent history. Human-induced land use/land cover changes during the latter half of the twentieth century coincided with major shifts in affluence, technological capacity, and socioeconomic organization (Meyer and Turner, 1992). In addition, a series of socio-economic and biophysical factors have been shown to affect the rate of change and spatial distribution of land use/land cover (Tayyebi et al., 2008). Therefore, major changes in land use/land cover may be expected, if the Sahel shifts from an agriculture-based economy to an industrialized system, especially if natural resource exploitation is intensified through the application of technological developments.

2.7 Geostatistical Methods in Land Use/Land Cover Change Detection

In order to measure and understand the nature of land use/land cover changes, a study area must be defined and the minimum effective spatial unit must be identified. The study area must be large enough to include a representative sample of all the variables analyzed and must have spatial continuity. The minimum unit of spatial observation in statistical analysis of a raster dataset is the grid cell, based on the assumption that any point located in the grid cell has the same value as the cell (Anselin, 1992). Therefore, for the development of the present study, the study area selected bounds 151,060.95 Square Kilometers of the basin of Lake Chad in northern Nigeria covering all the possible land use/land cover classes representative of the region, and the minimum grid cell resolution for each land use/land cover classification is the same as the grid cell size of the original satellite image.

Several methods may be used to interpret aerial photography and produce land use/land cover data for land use planning (Tayyebi et al., 2008). Comparing land use/land cover at different dates is the most commonly used method to detect a temporal change of land cover (Ouedraogo, 2010). In the present study, land use/land cover maps for 1970, 1986, 2000, 2005, and 2009 are analyzed using the post-classification method. This method was selected because studies demonstrate that post-classification land use/land cover analysis is more helpful in studying the nature of variation than pre-classification approaches (Mubea, Mundia, and Kuria, 2011). In addition, results from this analysis are more effective in identifying the nature of land use/land cover changes, rather than just the areas undergoing change.

In the process of detecting land use/land cover changes in the landscape, the size and location of the raster grid cells should match the spatial configuration of the base data to

produce a relatively accurate implicit sampling of the underlying spatial process (Anselin, 1992). One of the limitations encountered in the present study relates to the extent of the study area. Practical statistical analysis can only be conducted for such a large area by resampling the coverage to produce a representative sample of each of the land use/land cover maps.

In land use/land cover trend analysis two important measures of change must be examined: net change and gross change. Net change represents the net difference in area modified between two time-periods for a particular land use/land cover class, whereas gross change represents the total area modified between two periods and it indicates the overall amount of aggregate change from increases and decreases of a specific land use/land cover class (Loveland and Acevedo, 2011). Net land use/land cover change can be easily summarized directly from the areas of the polygons or raster grids for each land use/land cover class (Mackenzie, 2009). The calculation of gross land use/land cover change is not as straightforward. Gross changes may be calculated with the ArcGIS Tabulate Area tool, which produces a pairwise combination of land use classes for different time periods (Mackenzie, 2009). This gross change calculation aggregates area losses and gains for each class in the land use/land cover grid. It is important to note that net change and gross change can have different spatial extents for the same land use/land cover class (Stehman and Wickham, 2006). Therefore, the comparison of land use/land cover net and gross changes requires a geospatial representation.

In addition to summarizing net and gross land use/land cover changes, geostatistics can be used to calculate the accuracy of these measurements. Net change accuracy is nonsite-specific and targets a large support unit, whereas gross change accuracy is site-specific and

targets a per-pixel or per-polygon assessment (Stehman and Wickham, 2006). Gross change accuracy can be calculated using an error matrix of all the possible change transitions from one land use/land cover class to another between two different time periods (Stehman and Wickham, 2006). These metrics may be used to further analyze the results summarized in the present study.

In addition to quantifying land use/land cover change, a test for spatial autocorrelation of the coverage can be conducted through a GIS. Testing for spatial autocorrelation can help determine whether the set of observations presents a more significant spatial clustering pattern than what would be expected if the distribution was completely random, however, this test does not explain the nature of the clustering nor does it indicate the factors that influence the correlation's shape and strength (Anselin, 1992). In the present study, the Pearson's coefficient correlation equation was applied at multiple effective neighborhood sizes for each of the land cover classes, to identify areas of strong positive or negative autocorrelation.

A description of the spatial pattern of change for land use/land cover and population can be summarized through the use of indicator semivariograms that show the degree of spatial dependence of the underlying process. These tools can be used to study variables that change over time and space (Brown et al., 2002). In addition, comparing the degree of spatial and directional dependence between variables can help in the determination of the overall impact of population density on land use/land cover change.

2.8 Relevance of the Study

Advances in GIS and the ease of acquisition of satellite imagery through remote sensing facilitate the analysis of land use/land cover transitions in areas otherwise inaccessible to

investigators. Land use/land cover change assessments for rural areas of Africa developed through satellite remote sensing are more effective, relatively inexpensive, and faster to produce than monitoring assessments produced through the use of traditional surveys and inventories (Mubea, Mundia, and Kuria, 2011). Therefore, the geostatistical analysis presented in the present study is a cost-effective methodology to approach land use management and planning.

Regarding human population growth and land use/land cover change, Meyer and Turner (1992) reaches three important conclusions:

1. The forces that cause positive or negative land use/land cover change in a particular class may have an opposite effect on a different class.
2. Equal land use/land cover changes may be caused by different forces in different areas, even at regional micro-scales.
3. There is no agreement on the level to which a land use/land cover change can be attributable to a specific force, considering that several forces may be at play simultaneously.

Taking into consideration these guidelines, a detailed study of land use/land cover change and population density in the study area is presented in the following chapters.

CHAPTER 3

DATA SOURCES AND PRE-PROCESSING

In order to develop a solid geostatistical analysis of the study area, three variables were examined: climate and precipitation, satellite imagery, and population density. The native formats of these datasets varied depending on the spatial coverage, age of the information, or source of the data. Processing these datasets for analysis required extensive computer software use and customization of existing applications.

Four types of software were used to perform the statistical analyses described in the present study. The database software Microsoft Access[®] 2010 was used to design database schemas and custom queries for tabular datasets. Grapher[™] 9 and Surfer[®] 10, developed by Golden Software, were used to produce rose diagrams and indicator variograms respectively. ArcMap 10.0, under the ArcView license, was used to develop a Geographic Information System (GIS) to store, manage, and analyze all the geospatial data acquired and produced for the study area.

The following section summarizes the data types acquired, source, geospatial and temporal coverage, and analytical processes applied to describe the nature of these datasets. The datasets acquired and analyzed include: historical climate and precipitation records; georectified satellite imagery; pre-classified land use/land cover raster images and shapefiles; and, population density raster images.

3.1 Historical Climate and Precipitation Data

Historical climate and precipitation data for the study area was obtained from the National Oceanic and Atmospheric Administration's National Climatic Data Center (NOAA, 2011). Raw data tables were downloaded in comma separated value (CSV) format for 20

stations (Table 3.1) in the vicinity of the study area. The raw data tables contain the geographic coordinates for each station; monthly mean, minimum and maximum temperatures; monthly mean barometric pressure; and total monthly precipitation records.

Table 3.1. Stations with Historical Climate Data Available.

Station ID	Station Name	Country	Coordinates
60611	In Amenas	Algeria	28°03'N 9°38'E
60680	Tamanrasset	Algeria	22°48'N 5°26'E
64870	Ngaoundere	Cameroon	7°21'N 13°34'E
64700	Ndjamena	Chad	12°08'N 15°02'E
64706	Moundou	Chad	8°34'N 16°04'E
64751	Ati	Chad	13°13'N 18°19'E
64753	Faya	Chad	18°00'N 19°10'E
64754	Am-Timan	Chad	11°02'N 20°17'E
64459	Impfondo	Congo	1°37'N 18°04'E
62124	Sebha	Libya	27°01'N 14°27'E
62271	Kufra	Libya	24°13'N 23°18'E
61017	Bilma	Niger	18°41'N 12°55'E
61024	Agadez	Niger	16°58'N 7°59'E
61043	Tahoua	Niger	14°54'N 5°15'E
61096	Maine-Soroa	Niger	13°14'N 11°59'E
65123	Minna	Nigeria	9°37'N 6°32'E
65167	Yola	Nigeria	9°14'N 12°28'E
62760	El Fasher	Sudan	13°37'N 25°20'E
62770	Geneina	Sudan	13°29'N 22°27'E
62880	Wau	Sudan	7°42'N 28°01'E

Climate data available through the Climatic Data Center dates back to the year 1900, but it does not include information for certain weather stations located in the study area.

Therefore, in order to produce a more robust dataset, precipitation data for three additional stations (Lee et al., 2012) was incorporated in this analysis. Table 3.2 lists the weather stations that were selected for this analysis and the respective source for each data set.

Table 3.2. Precipitation Data Source by Station.

Station Name	Country	Source
Kano	Nigeria	Lee et al., 2012
Maiduguri	Nigeria	Lee et al., 2012
Maine-Soroa	Niger	NOAA, 2011
Minna	Nigeria	NOAA, 2011
Ndjamena	Chad	NOAA, 2011
Nguru	Nigeria	Lee et al., 2012
Tahoua	Niger	NOAA, 2011
Yola	Nigeria	NOAA, 2011

3.1.1 Data Assembly into a Database

In order to organize and analyze historical climate data, raw data tables for each country were imported to Microsoft[®] Access software and stored in a database. A union query was created in order to join all the data tables and standardize the results. A summary of total precipitation by year was queried for the eight stations in the vicinity of the study area. A map of the locations of these weather stations is provided in Figure 3.1.

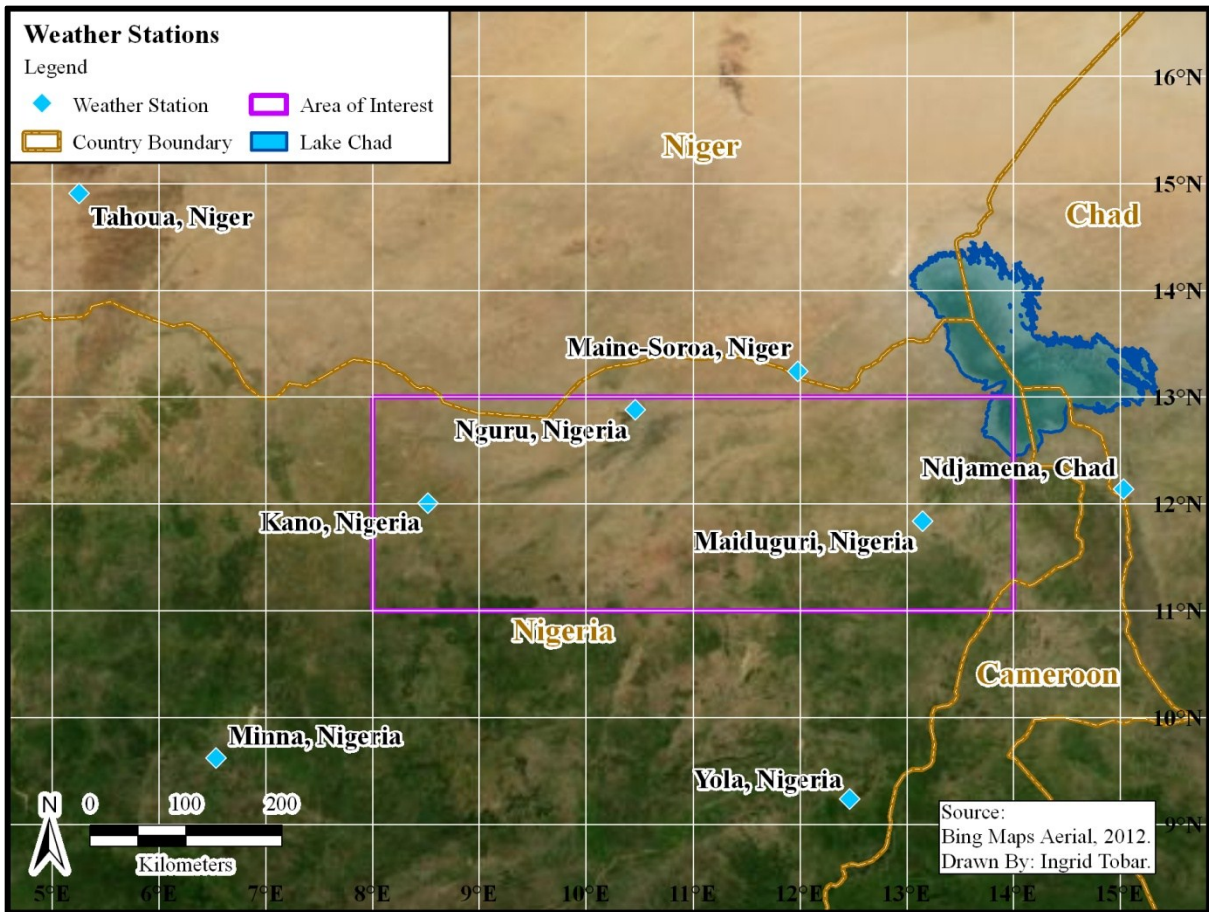


Figure 3.1. Weather Stations Near the Study Area

3.2 Satellite Imagery

Two sets of mosaicked satellite imagery were obtained from the U.S. Geological Survey's Global Visualization Viewer (USGS, 2010). This online resource provides public access to recent imagery captured by the ASTER (Advanced Spaceborne Thermal Emission and Reflection Radiometer) instrument of the Terra satellite, and historic imagery captured by the Earth observing instruments of various Landsat satellites. Landsat satellites 4 and 5 were equipped with Thematic Mapper (TM) instruments; whereas Landsat 7 was equipped with the Enhanced Thematic Mapper Plus (ETM+) instrument (NASA, 2011).

Due to the vast extent of the study area, existing satellite imagery mosaic tiles for two different time periods were further merged from individual tiles using the “Mosaic” tool of the Data Management toolbox in ArcGIS software. The first set of images consisted of two TM tiles derived from 1986 Landsat imagery (Figure 3.2). The second set consisted of six ETM+ tiles derived from imagery acquired between the years 1999-2003 (Figure 3.3).

Since the temporal coverage of the 1999-2003 satellite images spans only four years, the assumption is made that the mosaic of these images closely depicts the landscape of the study area in the year 2000, therefore, this data source and its derived products will be referred to as ‘2000’ throughout the present study.

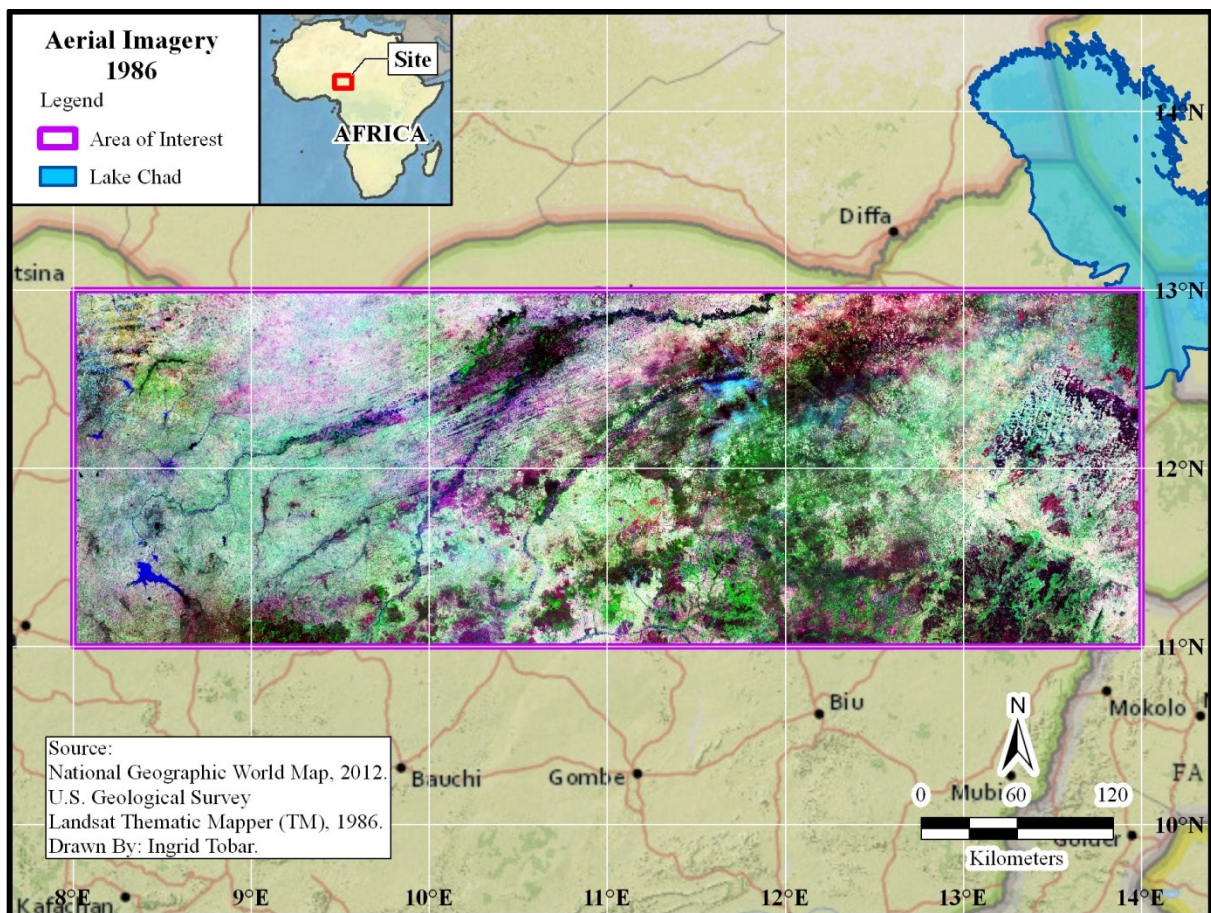


Figure 3.2. Landsat Thematic Mapper (TM) Satellite Imagery for 1986.

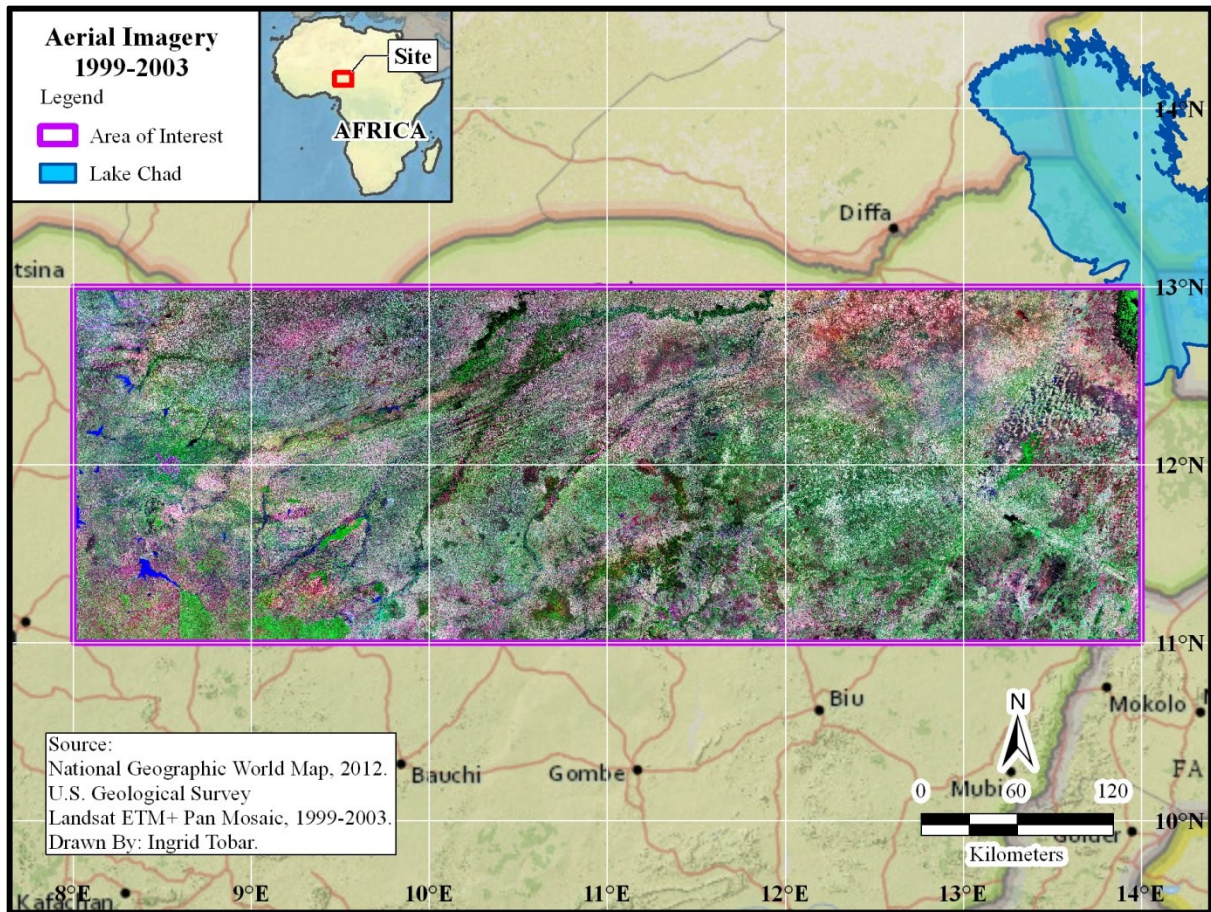


Figure 3.3. Landsat ETM+ Pan Mosaic Satellite Imagery for 1999-2003.

The westernmost 1986 satellite image for the study area was projected in the Universal Transverse Mercator (UTM) projection for zone 32 north, using the World Geodetic System (WGS) 1984, whereas the easternmost image was projected in zone 33 north. Four of the 2000 satellite images were projected in zone 33 north, but the two westernmost images were originally projected in zone 32 north. In order to standardize these datasets, all of the satellite images mosaics were reprojected to the World Mercator projection in the Geographic Coordinate System WGS 1984. Although this process may cause some

distortions and skewing of the original dataset inherent in the reprojection approach, this step was required in order to tabulate land use/land cover area summaries for the study area.

Furthermore, for ease of manipulation, the satellite image mosaics were clipped to the extent of the study area. The native spatial resolution of the 1986 satellite imagery was 30 m, whereas that of the 2000 satellite imagery was 15 m. The native spatial resolution was preserved to produce more accurate land use/land cover classification results.

3.2.1 Satellite Image Classification Process

In the present study, I merged two sets of Landsat tiles for 1986 and 2000 into separate images for each time period using the mosaic tool in ArcGIS software. Initially, the images were classified with an unsupervised classification method using the iso cluster tool of spatial analyst. The tool uses an isodata algorithm to determine the characteristics of the natural groupings of cells. However, this approach produced results that were not consistent with the patterns observed in the previously classified 1970s and 2009 land use/land cover raster images for the study area acquired from Lee et al. (2012). As a result a supervised classification approach was required in order to improve the quality of the results.

The supervised classification process required visually identifying sample locations of each land use/land cover class in the 1970s and 2009 raster images that coincided with particular landscapes in the 1986 and 2000 satellite images, and storing those sample points into separate shapefiles for the years in question: 1986 and 2000. Since the density of the sample points collected and their spatial distribution could affect the outcome of the classification process, careful selection of the sample points was important. The 1986 and 2000 original raster images and their respective land use/land cover sample point shapefiles were used to produce a new signature file for each of the satellite images. These new image

signature files were used to execute the maximum likelihood classification tool on the 1986 and 2000 satellite images to create a classified raster output. The results of this classification process were improved by including additional sample locations or reconfiguring their spatial distribution so that the final land use/land cover patterns for 1986 and 2000 would be consistent with those observed in the 1970s and 2009 classified raster images.

One of the disadvantages of the maximum likelihood classification tool is that it assumes that the classes in the input raster follow a Gaussian distribution and that it relies on the accuracy, in terms of value assignment and spacing, of the land use/land cover sample points selected from base raster images. Therefore, inadequate classification and/or distribution of the sample points may cause errors in the final classification of the satellite image. However, considering that the sample points selected were based on land use/land cover data pre-processed to guarantee accurate results, this method was the most effective approach to produce additional land use/land cover classification patterns consistent with the results obtained by ESA researchers.

3.3 Pre-classified Land Use/Land Cover Data

Pre-classified land use/land cover raster images for the 1970s and 2009 were obtained from Lee et al. (2012). The 2009 classified raster image, acquired by Lee et al. (2012) from the European Space Agency (ESA), was produced by applying various pre-processing techniques to a series of land surface reflectance mosaics. These techniques included geometric and atmospheric correction, cloud screening, shadow detection, land/water reclassification, and bidirectional reflectance distribution function (BRDF) effect reduction, among others (Lee et al., 2012). The 1970s classified raster was prepared from a mosaic of 1972-1979 Landsat images, using an unsupervised classification method based on the 2009

land use/land cover classes of the ESA classified raster image. This process ensured that the accuracy in land use/land cover distribution from the 2009 raster image was shared with the 1970s classified raster image.

In addition, a pre-classified land use/land cover dataset for the year 2005 was obtained from the GeoNetwork (FAO, 2011). The native file format of the 2005 land use/land cover classes was a polygon feature stored in a shapefile. The shapefile geometries covered the countries of Cameroon, Chad, Niger, and Nigeria. A GIS was used to merge the shapefiles, clip the combined coverage to the extent of the study area, and convert the polygon to a raster maintaining the original class value field in the output raster dataset.

3.4 Standardization of Land Use/Land Cover Classes

Table 3.3 summarizes the data sources and some of the properties of the original datasets. It is important to note that all the final land use/land cover raster images maintain the scale and resolution of their original raster datasets.

Table 3.3. Land Use/Land Cover Data Source Summary.

Temporal Coverage	Original Data Type	Resolution	Source
1970s	Landsat image	60m	Landsat Mosaic (Lee et al., 2012)
1986	Landsat image	28.5m	Landsat TM Mosaics
2000	Landsat image	14.25m	Landsat ETM+ Pan Mosaics
2005	Land cover shapefile	900m	GlobCover Regional (Africa) Archive
2009	Land cover classified coverage	300m	GlobCover 2009 Land Cover Map

The 1970s land use/land cover raster (Lee et al., 2012) was classified into ten distinct classes in accordance with the Anderson classification system (Anderson et al., 1976). The output raster image distinguishes the following land use/land cover classes: Rainfed cropland, mosaic cropland, mosaic vegetation, forest, shrubland, grassland, sparse vegetation, vegetation regularly flooded, bareland or urban area, and water body.

The land use/land cover class samples extracted from the 1986 and 2000 satellite images to create an updated signature file were selected taking into consideration these ten land use/land cover classes. The output from the Maximum Likelihood Classification process inherited these categories from the signature file.

The 2005 and 2009 pre-classified land use/land cover raster images required reclassification into the same standard classes used by Lee et al. (2012) in the 1970s dataset. The reclassification processes applied to the 2005 and 2009 raster images follows the reclassification system summarized in Table 3.4.

The end products of the classification process are four distinct land use/land cover raster images for the years 1986, 2000, 2005 and 2009, classified into the ten standard classes used by Lee et al. (2012) in the 1970s dataset.

3.5 Population Density

Population density for the African continent, for the years 1960, 1970, 1980, 1990, and 2000, was obtained from the Global Resource Information Database (UNEP, 2011).

Population density for the year 2010 was available through the Socioeconomic Data and Applications Center (SEDAC, 2011). These raster image datasets, derived from the African population database, were processed in a GIS for further analysis (Figure 3.4).

Table 3.4. Land Use/Land Cover Reclassification Scheme.

Original Classification		Reclassification Grouping	
Class	Description	Class	Description
11	Irrigated croplands	14	Rainfed Cropland
14	Rainfed croplands		
20	Mosaic croplands/vegetation		
30	Mosaic vegetation/croplands		
40	Closed to open broadleaved evergreen or semi-deciduous forest	110	Forest
50	Closed broadleaved deciduous forest		
60	Open broadleaved deciduous forest		
70	Closed needleleaved evergreen forest		
90	Open needleleaved deciduous or evergreen forest		
100	Closed to open mixed broadleaved and needleleaved forest		
110	Mosaic forest-shrubland/grassland		
120	Mosaic grassland/forest-shrubland		
130	Closed to open shrubland		
140	Closed to open grassland		
150	Sparse vegetation	130	Shrubland
160	Closed to open broadleaved forest regularly flooded (fresh-brackish water)	140	Grassland
170	Closed broadleaved forest permanently flooded (saline-brackish water)	150	Sparse Vegetation
180	Closed to open vegetation regularly flooded	180	Vegetation Regularly Flooded
190	Artificial areas		
200	Bare areas		
210	Water bodies	200	Bareland or Urban Area
		210	Water Body

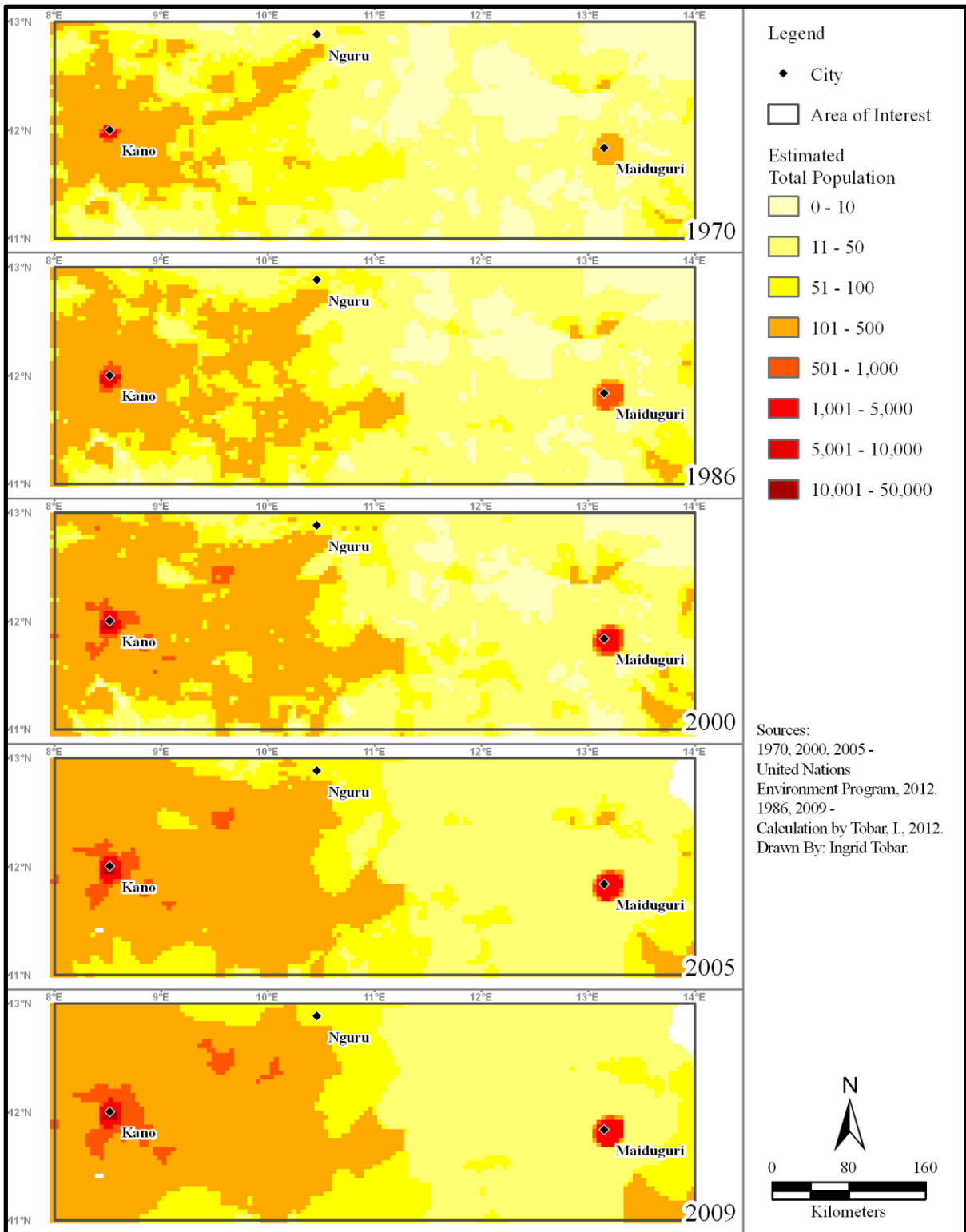


Figure 3.4. Population Density.

The original population density datasets covered the African continent and were saved in TIFF (Tagged Image File Format) format using the GCS Clarke 1866 Coordinate System. In order to standardize these datasets to match the theme of the land use/land cover data, the TIFF files were converted to GRID format (raster data storage format), and reprojected to the World Mercator projection in the Geographic Coordinate System WGS 1984. Lastly, all the population raster images were clipped to the extent of the study area.

Since the land use/land cover datasets available included the years 1986, 2005, and 2009, for which exact population records are not available, the population densities for these years were approximated assuming a linear growth pattern between each time period. This calculation was done by taking the difference of the population raster images available for the time period preceding and succeeding the year in question. The difference raster image was divided by 10 (the number of years separating the two original raster images) to produce a population density change raster image equivalent to the change observed in one year. To approximate the population density of a certain year between the two time periods, the raster image of the earlier period was added to the number of iterations of the yearly time-step raster as needed to reach the year in question.

For example, to approximate the population density of the year 1986, the difference between the population densities of 1980 and 1990 was calculated. The result was then divided by 10 (the number of years between the two periods), multiplied by 6 (the number of years between 1980 and 1986) and added to the original 1980 population density raster image. The disadvantage of this approach is that it produces a linear growth pattern between two time periods based on net changes and it does not account for gross change variability. However, in the case of population density, this type of approximation is reasonable because

this variable is not characterized by extreme changes from one period to the next and the linear approximation time steps span only 10 years.

3.5.1 Cell Size Limitations

The cell size of a raster image determines the spatial resolution of the raster and therefore the level of detail that can be represented in the image. After conversion to GRID format and reprojection, the cell size of the population density raster images is about 4.67 Kilometers, with cells arranged in a grid of 144 columns and 50 rows. Compared to the largest cell size in the land use/land cover dataset, which is 300m, this cell size is significantly larger and implies potential data loss in comparing the two datasets.

Cell size is the limiting factor in the direct analysis of correlations between population density and land use/land cover. The limitations inherent to the cell size of the population density dataset play an important role in the results obtained through the moving window simulated Pearson's correlation analysis described in Chapter 4. This justified the need to apply a different correlation analysis that could be conducted independently for the two variables and later combined for analysis. As a result, the variogram and rose diagram analyses were applied to achieve this goal.

CHAPTER 4

GEOSTATISTICAL ANALYSIS METHODOLOGY

This section describes the geostatistical analysis methods employed in the present study, which include interpolation techniques to approximate geospatial distribution of variables, correlation analyses to identify self-similarity in a variable and its relationship with other variables, and indicator variograms paired with rose diagrams to identify the degree and direction of spatial correlation of a variable.

4.1 Kriging Interpolation

Kriging interpolation is a function included in the spatial analyst toolset of ArcGIS software. The kriging process is a simple interpolation method and it assumes that the mean of the observations is relatively constant. This operation requires a geospatial point feature input with values associated with it to create a raster surface of the process investigated. In the present study, kriging interpolation was used to generate raster surface images of the spatial distribution of precipitation, based on records from eight weather stations located in the cities of Kano, Maine-Soroa, Maiduguri, Minna, Ndjamena, Nguru, Tahoua, and Yola.

For the given data distribution of these weather stations, the application of a kriging interpolation is appropriate. However, surface conditions may vary greatly between weather stations and caution must be exercised in the interpretation of this data. In the scope of this study, the kriging interpolation of precipitation data was conducted to compare the rainfall distribution patterns over the study area between different time periods, and in this manner, to identify potential periods of significance and important distribution changes in particular zones of the study area.

4.2 Spatial Autocorrelation

The Spatial Statistics toolset of ArcGIS includes a module for pattern analysis known as Spatial Autocorrelation (Global Moran's I). This function calculates the degree of spatial autocorrelation of an input raster based on the distribution of features and their attribute values. This tool can help analysts determine whether the distribution of the features and attributes investigated is dispersed, clustered or random, as described in Figure 4.1.

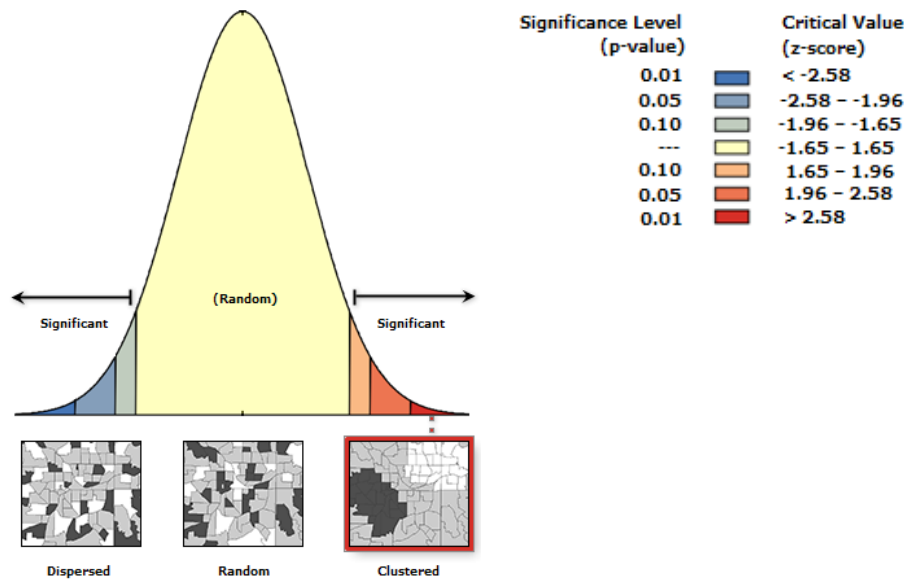


Figure 4.1. Spatial Autocorrelation Distribution and Significance Levels.

This test generates five metrics: the Moran's I Index, Expected Index, Variance, Critical Value (z-score), and Significance Level (p-value). The z-score and p-value indicate statistical significance and determine whether the null hypothesis may be rejected. The null hypothesis assumes that the distribution of the variable is random, neither clustered, nor dispersed. When either the z-score or p-value show statistical significance, a positive Moran's I Index indicates that the variable is clustered; whereas a negative Moran's I Index indicates a dispersed pattern (Moran, 1950).

4.3 Overlapping Neighborhood Statistics with Correlation Coefficient

In statistics, the Pearson's correlation coefficient between two variables can be calculated by finding the product of the covariance of each variable, and dividing that value by the product of the standard deviation of the variables. The calculated Pearson's correlation coefficient is represented with the Greek letter ρ (rho) and the formula is defined as:

$$\rho_{X,Y} = \frac{\text{cov}(X, Y)}{\sigma_X \sigma_Y}$$

where X and Y are the variables, cov is the covariance and σ is the standard deviation.

This formula was applied to find the Pearson's correlation coefficient between the land use/land cover and population density raster images. However, in the scope of this analysis, an overlapping neighborhood statistics component was incorporated so that the Pearson's correlation coefficient would include the effects associated with the spatial distribution and autocorrelation of the variables.

A four-module Overlapping Neighborhood Statistics Toolbox was developed in ArcGIS (Figure 4.2). The first module standardizes the raster images and their extent by excluding the combined locations of null values from the original raster images. Then it renames the raster images as X and Y for ease of manipulation. The second module computes the squares of the X and Y raster images, and their product. The third module computes the focal statistics of the outputs of the first and second modules. Since the focal statistics of a cell are calculated from the values within a specified neighborhood around it, the third module was subdivided into 4 sub-modules for the neighborhood cell sizes 3x3, 5x5, 7x7 and 10x10. The fourth module produces the standard deviation and covariance of the X and Y raster images, and uses these values to calculate the Pearson's correlation coefficient of the variables.

Module Number and Name

- Overlapping Neighborhood Statistics Toolbox
1. Standardize Grids X and Y
 2. Calculate Grids XX, YY, XY
 - 3a. Focal Statistics 3x3
 - 3b. Focal Statistics 5x5
 - 3c. Focal Statistics 7x7
 - 3d. Focal Statistics 10x10
 4. Pearson's Correlation Coefficient

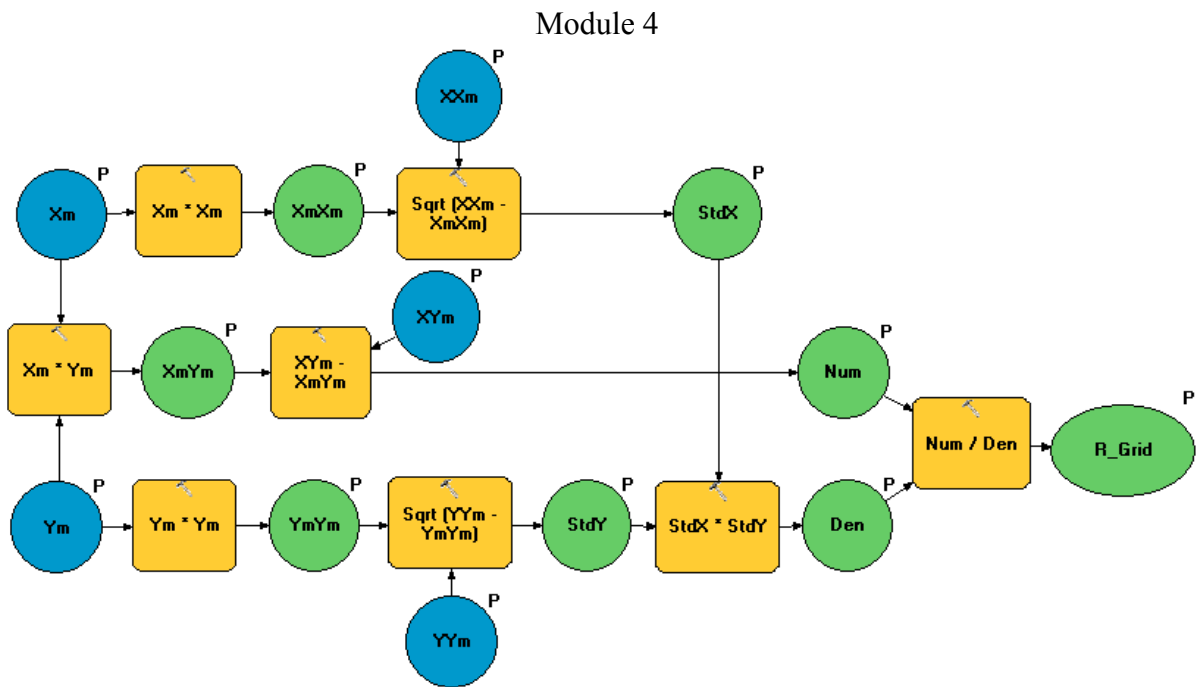
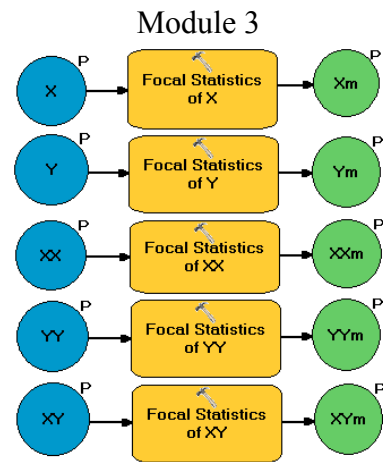
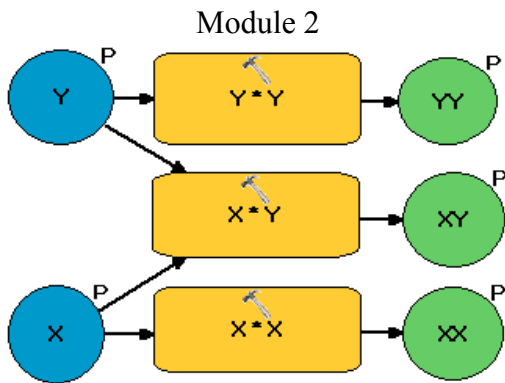
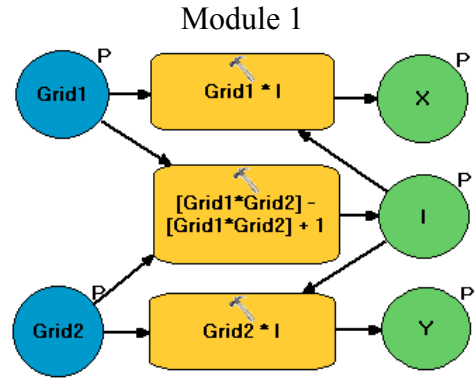


Figure 4.2. Overlapping Neighborhood Statistics Toolbox Modules.

4.4 Variogram Plots and Rose Diagram Analysis

In geostatistics, the variogram function describes the degree of spatial correlation of sample locations of a particular process. It is based on the first law of geography which establishes that correlation is stronger between neighboring sample locations than between those located further apart (Tobler, 1970). The variogram function is written as:

$$2\gamma(h) = \frac{1}{n} \sum [g(x) - g(x+h)]^2$$

where, h : separation or lag distance between data points,

n : number of data point pairs,

x and $x+h$: locations where a measure (g) was taken,

g : measured value at a specific location.

The variogram is normally plotted as a curve whose shape is defined by the presence of larger squared differences between distant samples than between neighboring samples (Figure 4.3).

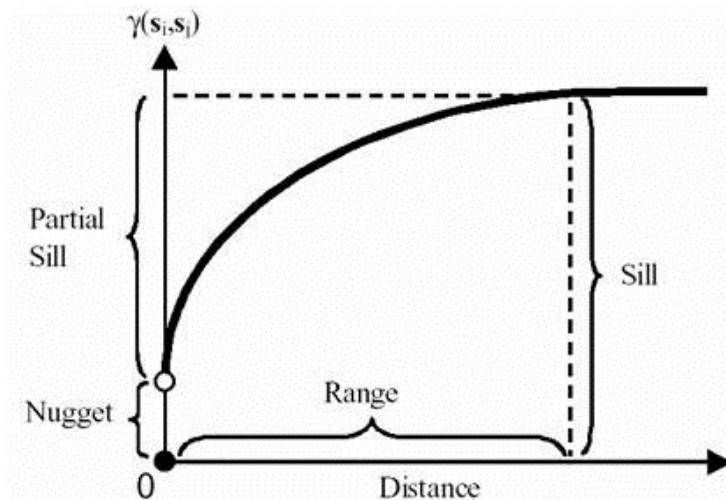


Figure 4.3. General Shape of the Semivariogram Function.

Three parameters define the variogram function: the nugget, which represents sub-grid scale variation or measurement errors and it is found at the y-intercept of the curve; the sill, which is the maximum semivariance value observed as the lag value (h) tends to infinity; and the range, the scalar that controls the degree of correlation between the data points (Clark, 1979).

The range is the most important parameter of the variogram function because it defines the maximum separation distance between observations for correlation effects to be detected. In other words, points located at a separation distance greater than the range are so distant that they are no longer related to each other and the values they represent are independent of one another. In the scope of this study, this value defines the maximum correlation distance between land use/land cover classes and population density values in the study area.

The Y axis of the variogram function shows the semivariance of the observations, and the X axis corresponds to the separation distance between the observations. The variogram function generally increases from the point of origin following a curve (circular, exponential, or Gaussian), reaches a maximum sill value and then tapers off.

Surfer[®] 10, developed by Golden Software, was used to plot the variogram function for six of the land use/land cover classes: rainfed cropland, mosaic cropland, mosaic vegetation, grassland, sparse vegetation, and vegetation regularly flooded. These classes were selected because they showed significant variability from one period of observation to the next. The population density raster images were analyzed in a similar fashion with this software.

Since the extent of the study area is relatively large, running the variogram function for every cell in the high-resolution raster images would extend the execution time of the software, therefore, a data reduction technique was put in place in order to expedite the

variogram calculation process and to obtain consistent results. In order to standardize the datasets prior to running the variogram function, the following sampling methodology was introduced: Starting at southwest corner of the study area (the point corresponding to 11° N latitude and 8° E longitude) sample points were taken with 1 Km vertical and horizontal separation distance throughout the extent of the study area, producing a grid of 151,863 evenly-spaced sample locations.

After these sample locations were defined, a shapefile feature class was produced for each of the raster images to be analyzed. For population density data, five shapefiles were created for each year studied (1970, 1986, 2000, 2005, and 2009). These shapefiles contained the XY coordinates of the sample locations and the population density value from the original raster image. Variogram plots for population density were calculated using the tabular data contained in these shapefiles, however, additional pre-processing was required for land/use land cover classes before the shapefiles could be generated.

Since the land use/land cover raster data included multiple classes in a single file, the classes had to be isolated from each other in order to produce indicator variogram plots for each class. Indicator variograms are normally used when the variables are binary or represent classes of values (Cressie, 1993). In the case of land use/land cover data, the original raster image was split into binary raster images for each of the classes investigated, where a cell value of 1 was assigned to the cells corresponding to the land use/land cover class in question, and all other cells were assigned the value of 0. After this process was completed, shapefiles were generated for each class in the same fashion as it was done for the population density dataset. Figure 4.4 shows a sample indicator map for the mosaic cropland class after it was converted to a binary raster image, and isolated from all other classes.

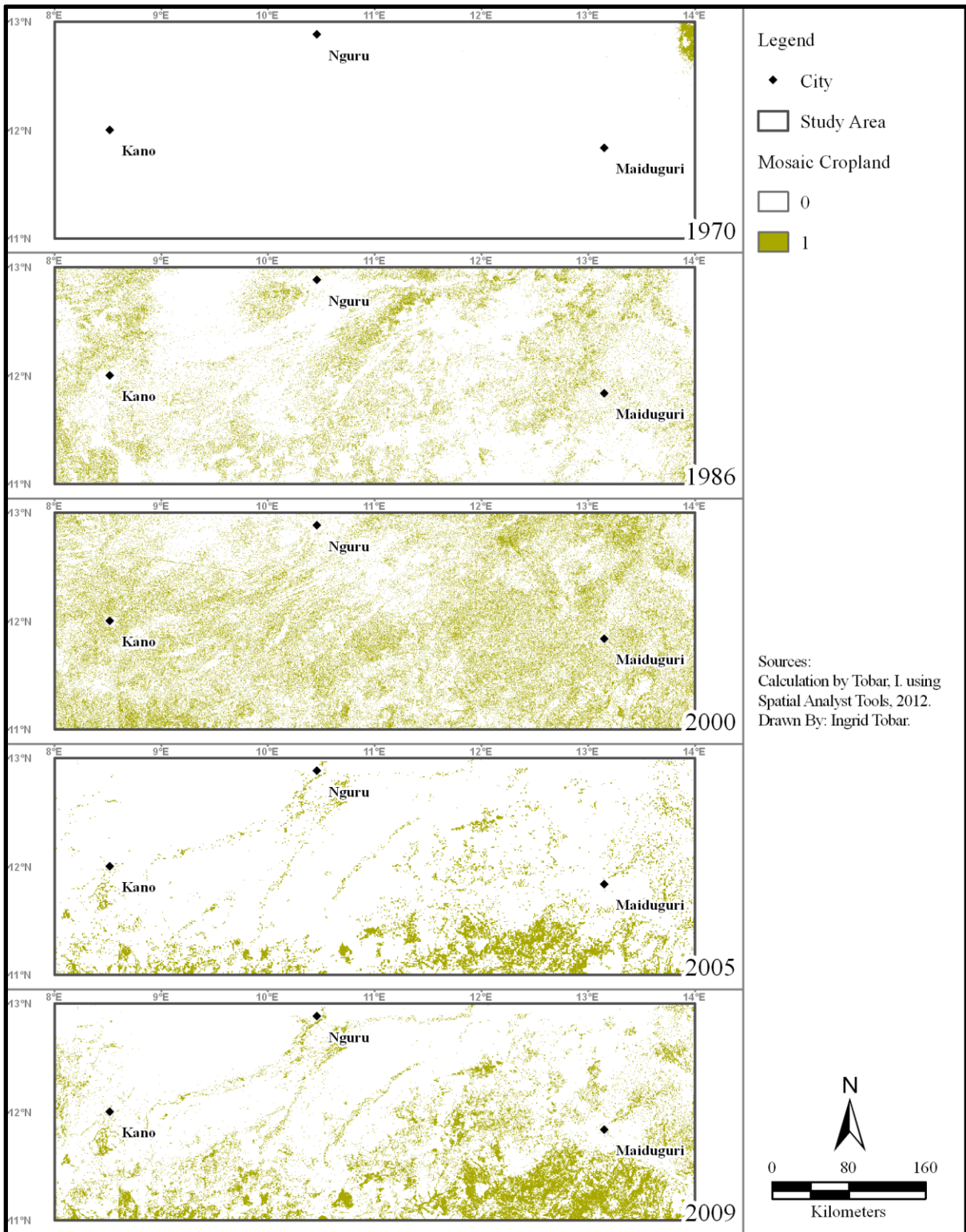


Figure 4.4. Sample Indicator Map for Mosaic Cropland Class Converted to Binary.

The tabular data stored in the shapefiles was converted to comma separated value (CSV) format and used as input for the variogram function of Surfer[®] 10 software, using a maximum lag distance of 6. The variogram function was plotted for each of the datasets in eight coordinate directions: 0°, 30°, 45°, 60°, 90°, 120°, 135°, and 150°; each with an angular tolerance of 20°. It is important to note that the focal direction observed by the Surfer[®] 10 software to run the experimental variogram is in the standard notation used in geostatistics, where 0° is along the positive X axis, and 90° is along the positive Y axis, and the direction is not given as an azimuth. Figure 4.5 shows an example of the variogram plots for the 1970 mosaic cropland land use/land cover class.

Since the variogram function was calculated for only eight coordinate directions, covering half of the plane, the range distances for the remaining half are assumed to be equal to the ranges found in the respective opposite coordinate directions of the plane. These ranges and coordinate direction angles were summarized in a table that was used to produce a rose diagram. This diagram shows the maximum range distance of sample correlation along a specific direction. In addition, the rose diagrams for each of the population density raster images were overlaid in the same graph with the land use/land cover classes to identify similarities in the extent of directional correlation for the two variables. The rose diagrams and the results observed are summarized in the next chapters of the present study.

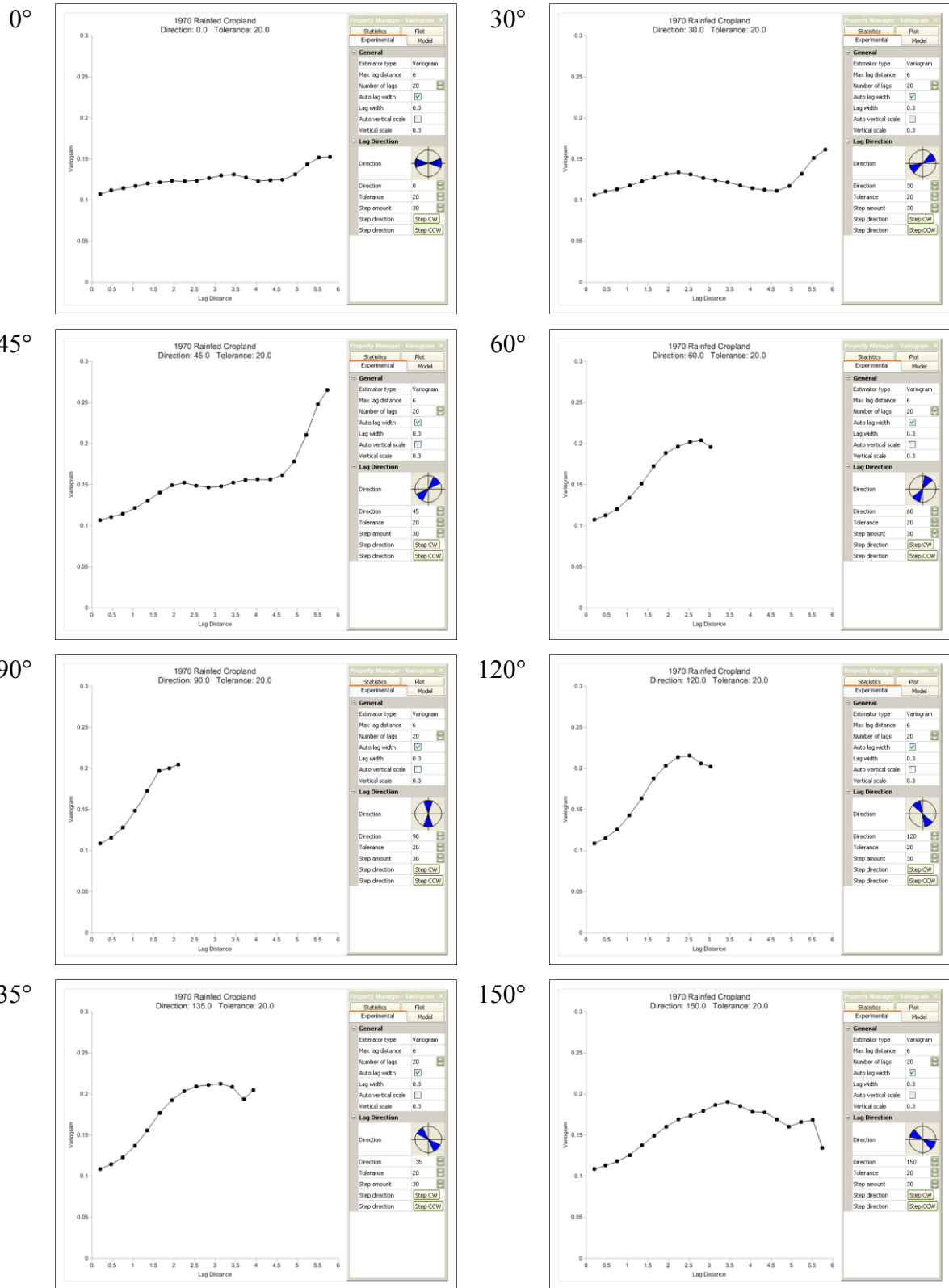


Figure 4.5. Example Variogram Plots for the 1970 Rainfed Cropland Class.

CHAPTER 5

RESULTS AND DISCUSSION

5.1 Precipitation Data

Two methods were used to summarize the historical precipitation data gathered for the study area. The first approach was to combine all the records into a database and extract yearly precipitation totals to plot a time-series for each weather station. The second method consisted of performing a kriging interpolation of yearly precipitation subsets to gain insight on the time period during which significant fluctuations occurred.

5.1.1 Time-Series Summary

Yearly precipitation records for Kano, available from 1974 to 2004, show an increasing precipitation trend. However, this result is inconsistent with the overall precipitation trends observed at the other seven stations near the study area. Yearly precipitation records for the other seven weather stations show a decreasing trend over the period 1970 to 2004 (Figure 5.1). This result is consistent with other studies that describe reduced precipitation trends in the region. Additional analysis of this trend is required in order to fully characterize the nature of these variations over time and their relation to land use/land cover changes.

5.1.2 Kriging Interpolation

The precipitation records summarized from the database were used to produce yearly precipitation distribution raster images through a kriging interpolation technique (Figure 5.2). The purpose of this exercise was to identify periods of extreme fluctuation in precipitation. This analysis shows that significant changes in precipitation occurred after 1980; therefore, this time period requires special attention since the changes in precipitation may also have a significant impact on land use/land cover transitions.

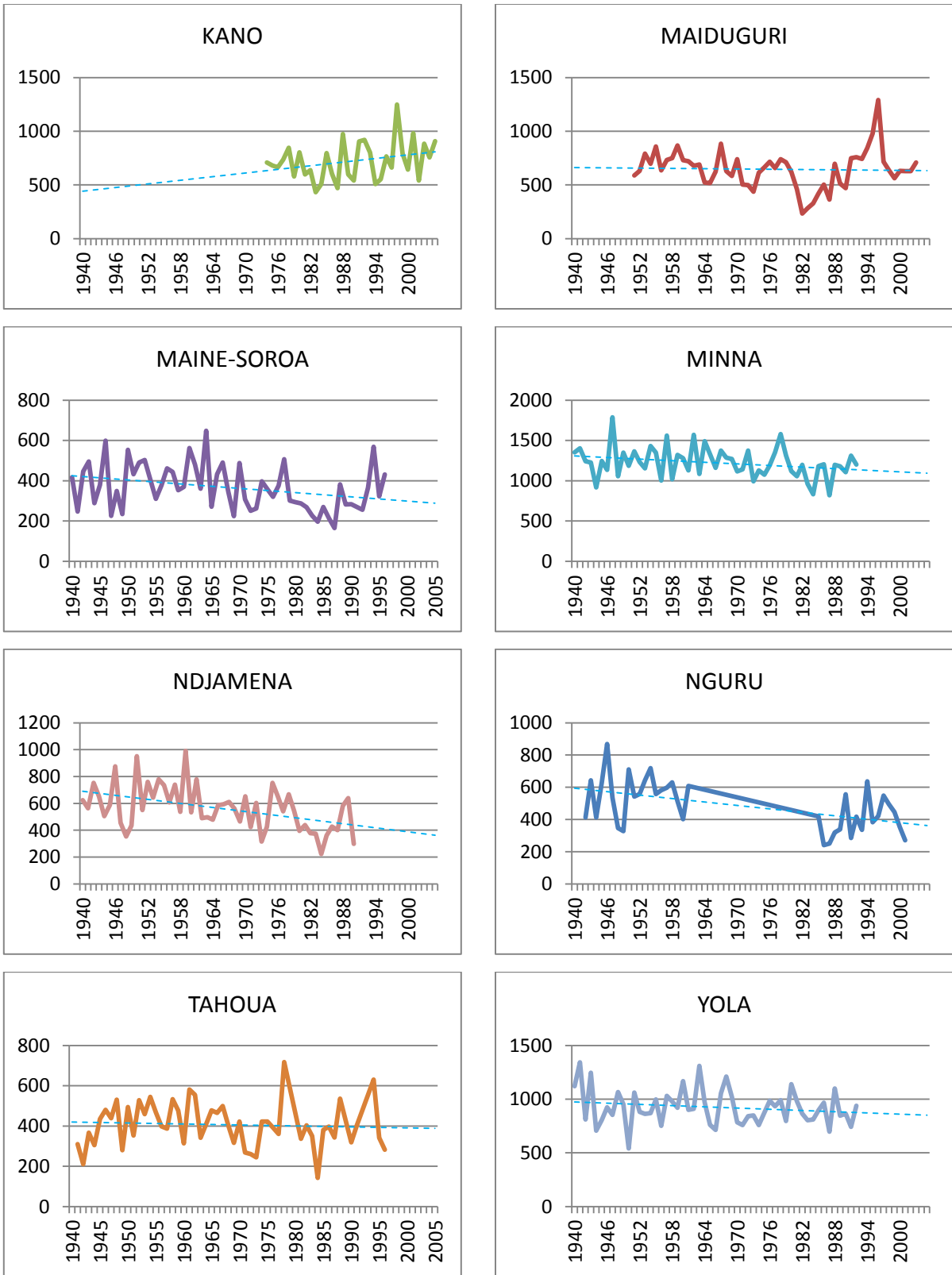


Figure 5.1. Yearly Precipitation Records for Weather Stations Near the Study Area.

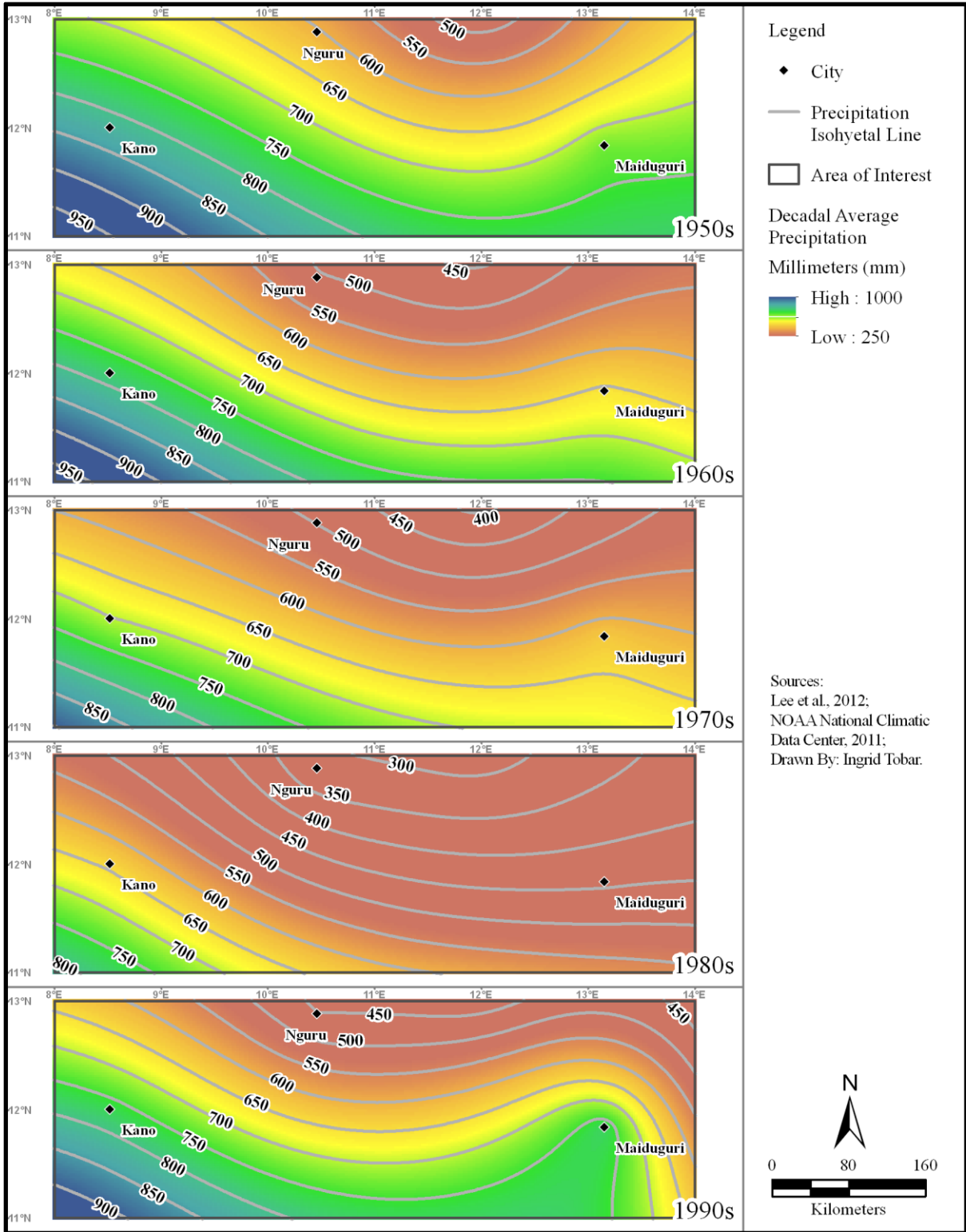


Figure 5.2. Decadal Average Precipitation Distribution in the Study Area.

5.2 Land Use/Land Cover

The land use/land cover classified raster images for 1986 and 2000 were assembled in a map (Figure 5.3) for visual inspection against the pre-classified land use/land cover datasets for 1970, 2005, and 2009. A summary of the area (in square kilometers) covered by each land use/land cover class in the datasets for these five years is provided in Table 5.1. This table was later used to calculate the net change in land use/land cover between consecutive time periods.

Table 5.1. Land Use/Land Cover Area Summary by Class and Year.

Class	Description	Area (km ²)				
		1970	1986	2000	2005	2009
14	Rainfed Cropland	23,862.41	9,568.40	50,491.10	43,847.73	43,089.93
20	Mosaic Cropland	519.01	19,389.35	37,506.02	13,102.56	22,662.00
30	Mosaic Vegetation	26,820.18	26,382.47	1,498.95	59,109.75	53,750.52
110	Forest	5,729.24	5,796.41	5,500.03	4,297.05	2,667.42
130	Shrubland	16,190.00	4,059.82	18,083.06	5,076.27	1,775.61
140	Grassland	10,184.00	18,845.34	7,463.59	23,608.26	24,207.03
150	Sparse Vegetation	28,050.70	15,139.04	11,889.50	660.96	2,047.59
180	Vegetation Regularly Flooded	20,611.08	30,158.93	15,708.03	148.23	117.99
200	Bareland or Urban Area	589.45	19,650.07	2,422.99	511.92	310.32
210	Water Body	14,168.53	2,104.49	508.80	492.48	427.95
	Total Area	146,724.59	151,094.31	151,072.05	150,855.21	151,056.36

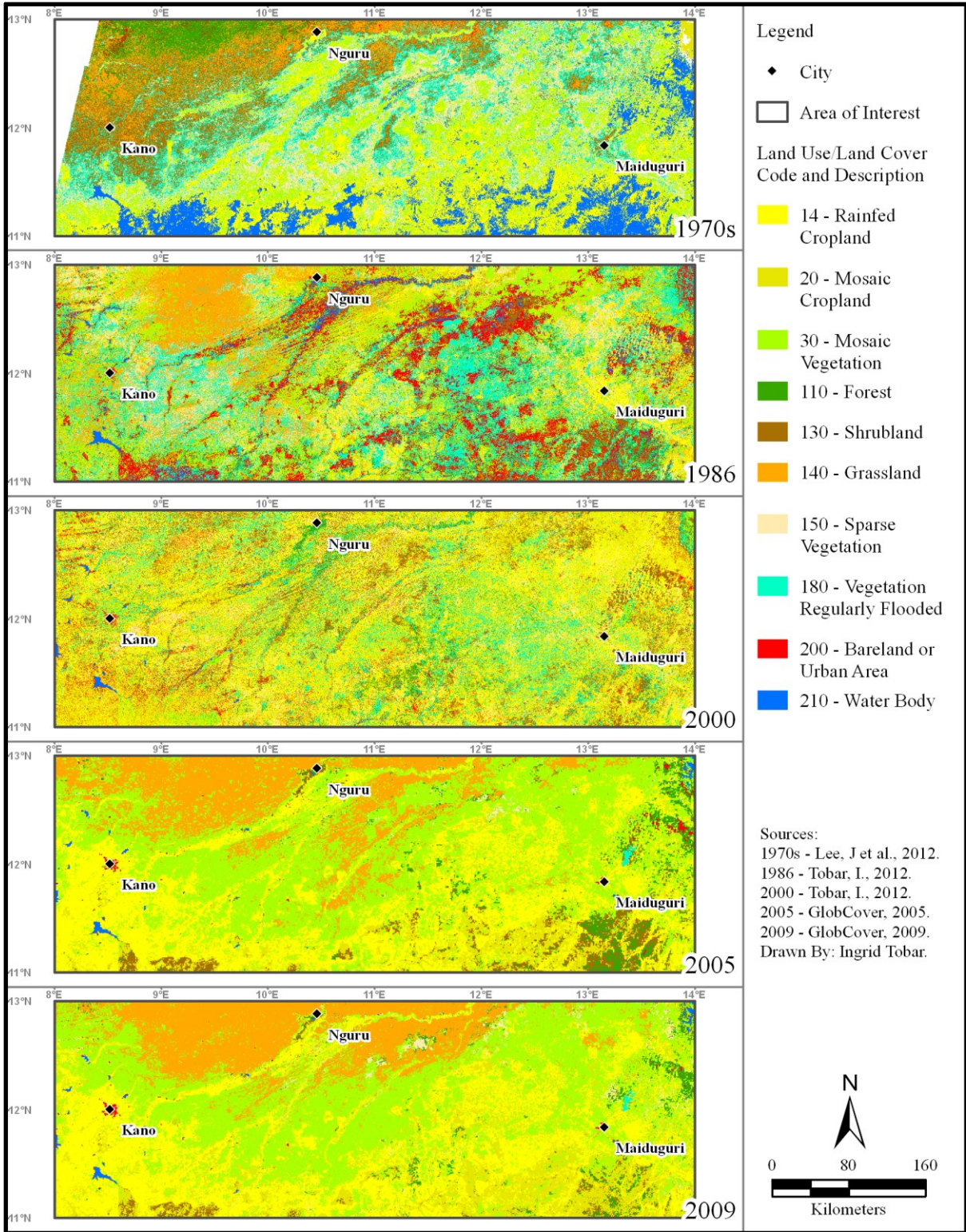


Figure 5.3. Land Use/Land Cover Classified Raster Images.

5.2.1 Percent Net Change

The scope of the present study was limited to the calculation of net changes in land use/land cover between two time-periods. The calculation of gross changes requires the development of probability transition matrices and due to time constraints this approach was not included. Table 5.2 and Figure 5.4 describe in detail the percent net change observed for each land use/land cover class between consecutive time periods. Based on these percent net changes six land use/land cover classes showing significant variation were selected for the variogram analysis. The classes selected include: rainfed cropland, mosaic cropland, mosaic vegetation, grassland, sparse vegetation, and vegetation regularly flooded.

Table 5.2. Land Use/Land Cover Percent Net Change.

Class	Description	% Net Change			
		1970 - 1986	1986 - 2000	2000 -2005	2005 - 2009
14	Rainfed Cropland	-9.93	27.09	-4.36	-0.54
20	Mosaic Cropland	12.48	11.99	-16.14	6.32
30	Mosaic Vegetation	-0.82	-16.47	38.19	-3.60
110	Forest	-0.07	-0.20	-0.79	-1.08
130	Shrubland	-8.35	9.28	-8.60	-2.19
140	Grassland	5.53	-7.53	10.71	0.38
150	Sparse Vegetation	-9.10	-2.15	-7.43	0.92
180	Vegetation Regularly Flooded	5.91	-9.56	-10.30	-0.02
200	Bareland or Urban Area	12.60	-11.40	-1.26	-0.13
210	Water Body	-8.26	-1.06	-0.01	-0.04

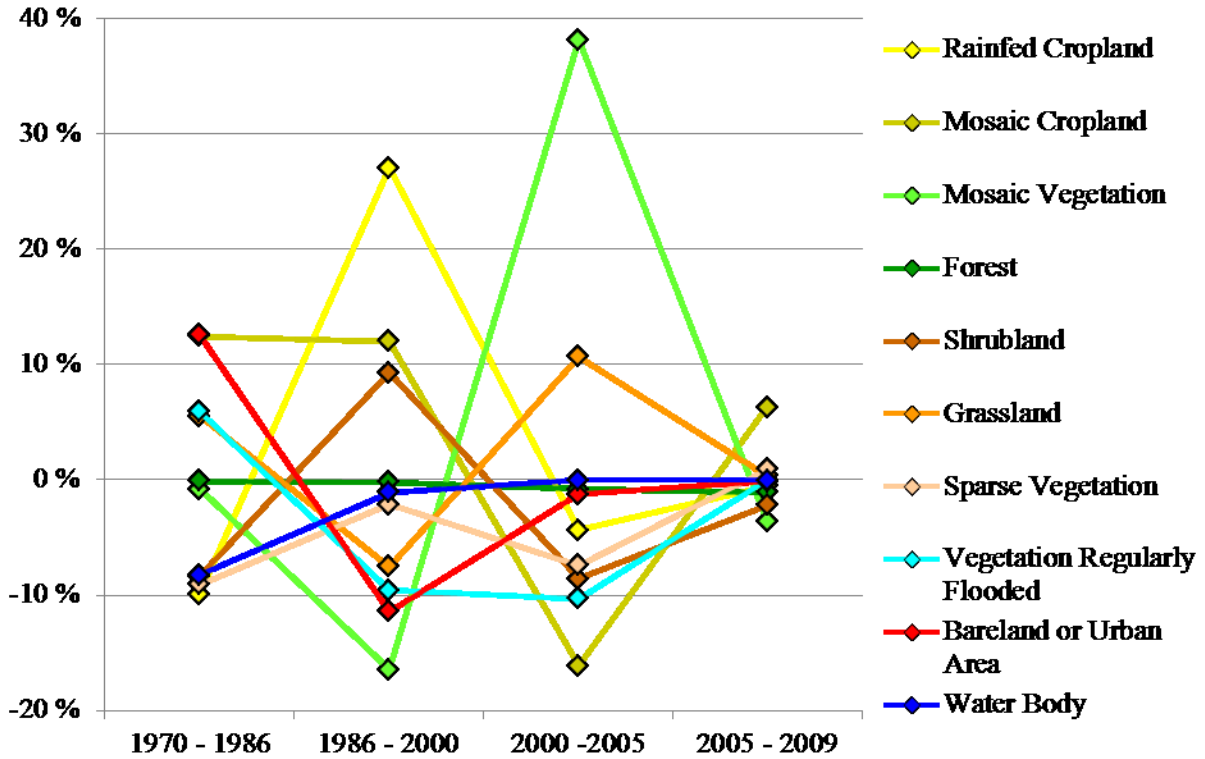


Figure 5.4. Land Use/Land Cover Percent Net Change.

5.2.2 Spatial Autocorrelation

The metrics obtained from the spatial autocorrelation test are summarized in Table 5.3. The Moran's I Index is positive for all the land use/land cover datasets, which indicates that the distribution of the land use/land cover classes is clustered. However, since all the Moran's I Index values obtained are close to zero, which would indicate a random spatial pattern, these values may be converted to z-scores to determine if the spatial autocorrelation of the variable analyzed is significant (Moran, 1950). Since all of the critical values (z-scores) obtained are greater than 2.58, I conclude that there is less than 1% likelihood that the clustered patterns could be the result of random chance. Therefore, the land use/land cover patterns observed in all the years examined display a certain degree of autocorrelation.

This result implies that agricultural expansion, increased urbanization, and the expansion of deserts, some of the most significant land use/land cover changes observed in recent years throughout the Sahel, tend to appear in the landscape in a spatially clustered fashion. The manner in which these land use/land cover classes propagate into areas previously covered with forests, wetlands, or natural environments requires further examination with more detailed geostatistical techniques.

Table 5.3. Spatial Autocorrelation Metrics.

Land Use/ Land Cover	Moran's I Index	Expected Index	Variance	Critical Value (z-score)
1970	0.169	-0.000003	0	586.396
1986	0.097	-0.000002	0	263.375
2000	0.011	-0.000002	0	33.118
2005	0.237	-0.000026	0.000001	208.111
2009	0.202	-0.000014	0	365.538

5.3 Population Density and Land Use/Land Cover

Two analyses were conducted in an attempt to identify relationships between population density and land use/land cover. The first approach consisted of calculating the Pearson's correlation coefficient of the variables incorporating the neighborhood statistics of the sample points. The second method required calculating the variogram function of each land use/land cover and population density raster image, and comparing the range values obtained from the variograms in a rose diagram.

5.3.1 Overlapping Neighborhood Statistics with Correlation Coefficient

The Pearson's correlation coefficients obtained through the overlapping neighborhood statistics tool are summarized in Table 5.4. These results show that the Pearson's correlation coefficient values lose significance for the land use/land cover raster images for 1986 and 2000 when the neighborhood cell size is greater than 7x7. However, the standard deviation values are smaller and more consistent among the different years of observation when the neighborhood cell size is 10x10. This indicates that the 10x10 neighborhood cell size would provide a more defined result of spatial correlation between the variables.

Table 5.4. Pearson's Correlation Results from Overlapping Neighborhood Statistics Tool.

Land Use/ Land Cover	Neighborhood Size: 3 x 3			Neighborhood Size: 5 x 5		
	Min	Max	Std Dev.	Min	Max	Std Dev.
1970	-1.000	1.001	0.386	-1.000	1.001	0.261
1986	-0.992	0.976	0.369	-0.800	0.707	0.238
2000	-0.990	0.974	0.369	-0.758	0.745	0.223
2005	-1.000	1.000	0.398	-1.000	1.000	0.272
2009	-1.000	1.008	0.390	-1.000	0.961	0.263
Land Use/ Land Cover	Neighborhood Size: 7 x 7			Neighborhood Size: 10 x 10		
	Min	Max	Std Dev.	Min	Max	Std Dev.
1970	-1.000	1.001	0.219	-1.000	1.001	0.188
1986	-0.628	0.639	0.188	-0.546	0.426	0.149
2000	-0.603	0.545	0.164	-0.388	0.454	0.119
2005	-1.000	0.992	0.221	-0.745	0.960	0.184
2009	-0.991	0.926	0.223	-1.000	0.844	0.201

Notes
Std Dev: Standard Deviation. Neighborhood sizes are in cell units.

The Pearson's correlation coefficients for each neighborhood cell size obtained through this calculation were plotted in a series of maps (Figures 5.5 – 5.8) for visual inspection, applying a stretched color ramp to the correlation values. In the areas shaded with red color a strong direct correlation between land use/land cover and population density was detected; the areas shaded with blue color show a strong inverse correlation between these variables; and, in the areas shaded with pale yellow color no correlation between the variables was detected.

Furthermore, a side-by-side comparison of the land use/land cover maps and the correlation coefficients obtained in this analysis is shown in Figure 5.9. This comparison shows that areas known to display increasing population density trends, such as the cities of Kano and Maiduguri, have a strong direct correlation with land use/land cover. In other words, as population density increases in these areas, the land use/land cover values also increase and tend towards values corresponding to less natural environments, such as bareland or urban areas.

In addition, inspection of the correlation map for 1970s shows a strong inverse correlation between population density and land use/land cover in the southern fringes of the study area. The population density in that region during the 1970s was low and the area was characterized by the presence of water bodies and vegetation regularly flooded. These land use/land cover classes were predominant while population density remained low, but they began to disappear in subsequent years. The same area also shows an inverse correlation, but not as strong in the 2005 map. However, this time, the inverse correlation is caused by high population density and rapid expansion of agriculture into the zone.

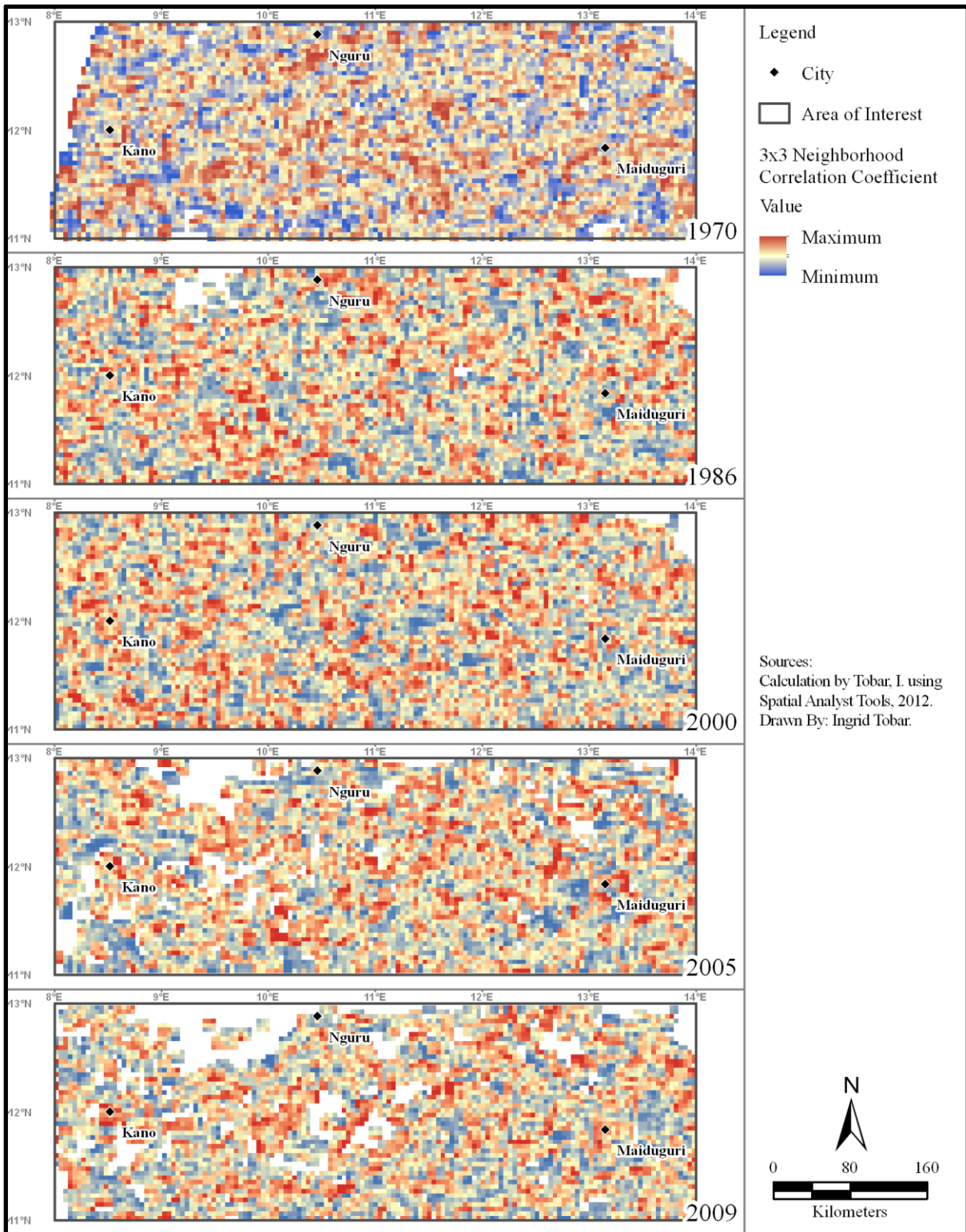


Figure 5.5. Correlation Coefficients for 3x3-Cell Overlapping Neighborhood.

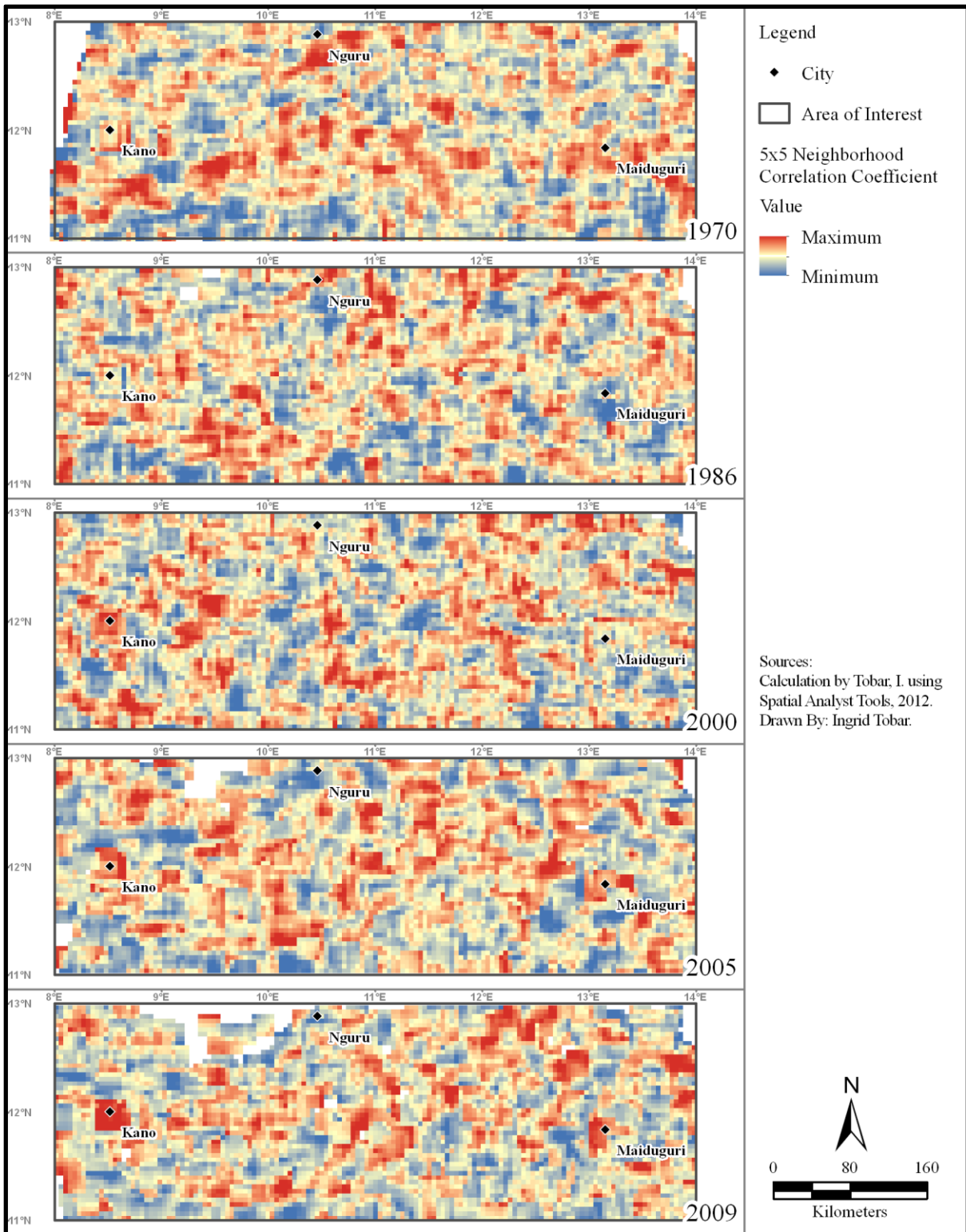


Figure 5.6. Correlation Coefficients for 5x5-Cell Overlapping Neighborhood.

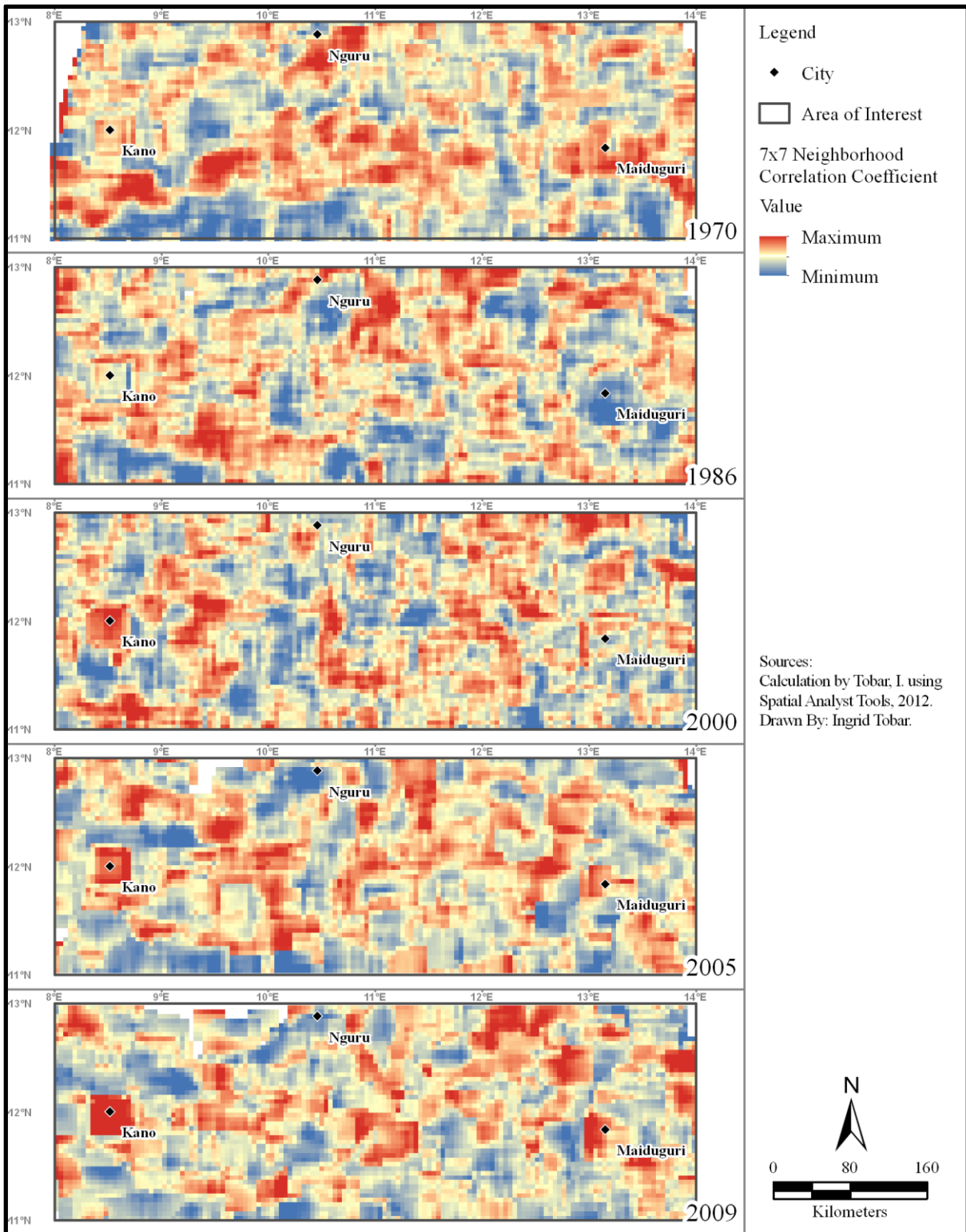


Figure 5.7. Correlation Coefficients for 7x7-Cell Overlapping Neighborhood.

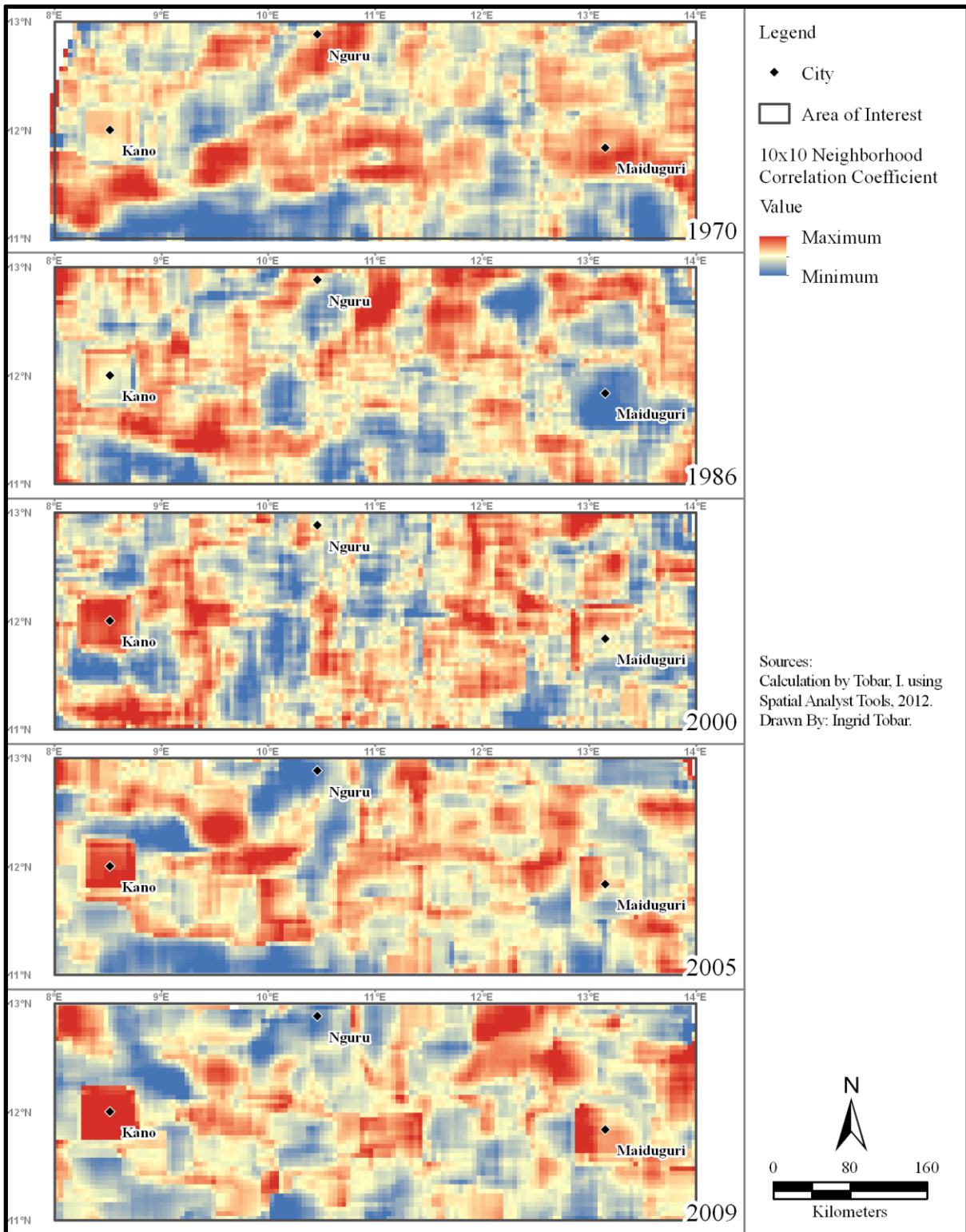


Figure 5.8. Correlation Coefficients for 10x10-Cell Overlapping Neighborhood.

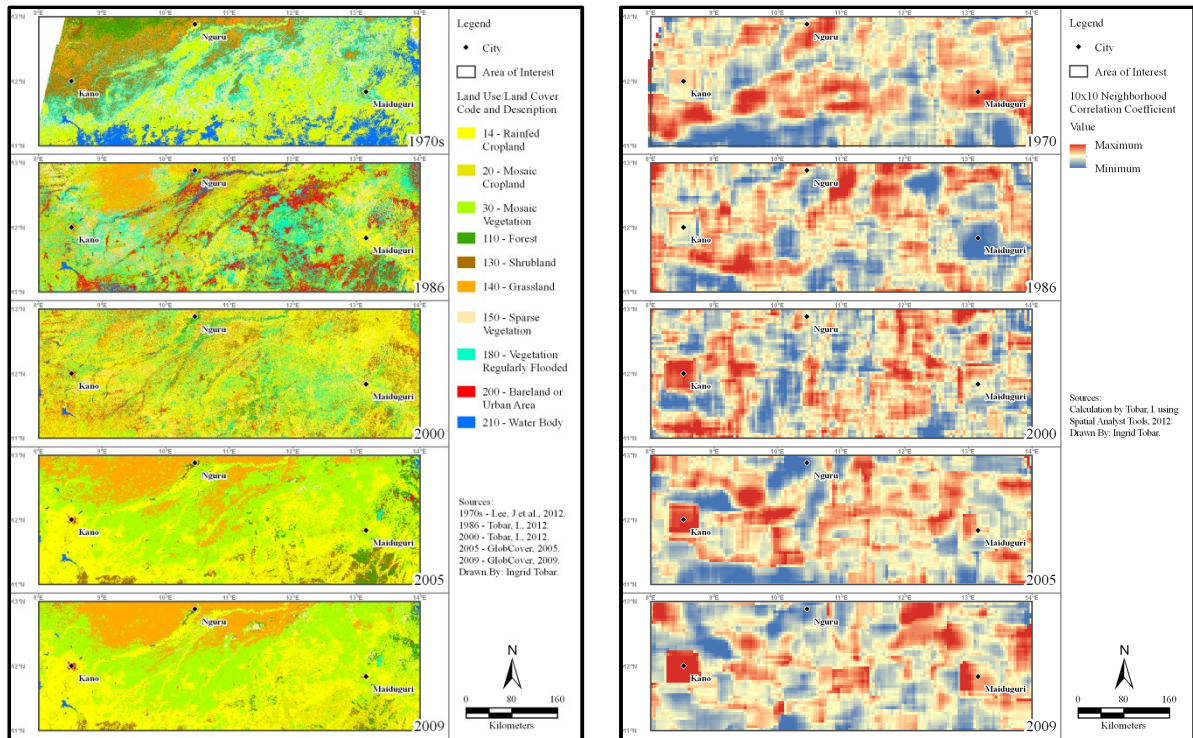


Figure 5.9. Side-by-side Comparison of Land Use/Land Cover and Correlation Coefficients.

5.3.2 Variogram Plots and Rose Diagram Analysis

Variogram plots were developed using Surfer[®] 10 software for six of the land use/land cover classes that showed significant variations between consecutive time periods, and for all of the population density raster images developed. The ranges of the variogram plots were recorded for eight coordinate directions (0°, 30°, 45°, 60°, 90°, 120°, 135°, and 150°) with an angular tolerance of 20° and summarized in Table 5.5.

These results were used to create rose diagrams using Grapher[™] 9 software for land use/land cover and population density raster images for each year covered in the scope of the present study. The rose diagrams for population density were plotted over the land use/land cover diagrams to in order to identify classes and directions for which spatial correlation ranges are similar between the two variables.

Table 5.5. Indicator Variogram Range Values.

Direction Angle	Population	Rainfed Cropland	Mosaic Cropland	Mosaic Vegetation	Grassland	Sparse Vegetation	Veg. Reg. Flooded
1970							
0	5.21	5.80	5.75	5.82	5.25	1.59	2.51
30	5.25	5.82	5.78	5.81	0.50	4.08	4.63
45	0.50	5.71	5.70	1.12	1.95	3.12	3.13
60	0.75	2.88	2.88	0.82	3.00	0.75	1.05
90	0.75	2.13	1.88	0.80	2.13	0.75	0.75
120	0.76	2.62	0.21	1.09	2.95	0.75	0.75
135	0.76	3.13	0.20	1.06	3.13	0.78	0.75
150	4.63	3.50	0.23	5.75	5.75	1.38	1.08
1986							
0	5.26	4.91	5.79	5.82	4.00	4.63	3.74
30	5.25	2.88	5.81	3.78	1.08	4.37	5.75
45	0.50	0.75	5.73	4.63	1.09	0.75	5.62
60	0.78	0.78	3.06	2.51	1.65	0.77	0.76
90	0.76	0.75	2.12	1.90	1.90	0.78	0.79
120	0.77	0.79	3.09	1.91	2.81	0.76	0.78
135	0.49	0.83	3.87	1.97	3.71	0.77	1.09
150	4.63	5.85	5.21	1.95	4.36	5.75	1.38
2000							
0	5.25	0.77	5.13	5.75	5.82	4.08	1.38
30	5.18	3.13	5.13	5.83	5.86	0.76	1.10
45	0.50	2.87	5.13	5.71	4.31	0.77	1.15
60	0.78	3.05	3.07	2.87	2.25	0.75	0.75
90	0.75	1.38	2.13	1.88	1.61	0.76	0.75
120	0.76	3.08	0.76	1.89	2.26	2.60	0.74
135	0.50	3.88	0.78	1.64	3.90	3.91	1.08
150	4.63	5.77	5.75	0.24	5.81	5.78	3.65
2005							
0	5.25	5.82	5.55	2.37	2.59	5.84	5.25
30	5.25	5.79	5.87	4.71	1.69	5.86	5.80
45	0.49	5.71	5.71	4.63	1.95	5.74	5.73
60	0.75	2.52	3.05	1.03	3.05	3.06	0.75
90	0.75	1.38	2.13	1.05	2.23	1.38	0.76
120	0.75	1.37	3.09	1.38	3.08	1.65	0.75
135	0.50	1.37	3.91	1.37	3.69	1.68	0.75
150	4.63	5.75	4.08	1.63	4.37	5.79	0.50
2009							
0	5.27	5.76	5.82	2.28	3.14	5.82	5.25
30	5.25	5.79	5.88	4.63	1.96	5.84	5.75
45	0.50	5.71	5.61	5.23	1.98	5.72	5.74
60	0.76	2.55	3.05	1.12	3.05	2.52	3.04
90	0.79	1.38	2.13	1.10	2.13	1.63	0.75
120	0.80	1.37	3.10	1.08	3.06	1.92	0.75
135	0.50	1.38	3.95	1.09	3.95	1.95	0.75
150	4.45	5.77	4.65	5.58	4.04	5.81	0.45

The rose diagrams are summarized in Figures 5.10 - 5.14. Visual inspection of the rose diagrams shows that the range values and direction of population density are similar to those of mosaic cropland (all years, except 1970); rainfed cropland (1970, 2005, and 2009); sparse vegetation (1986, 2005 and 2009); mosaic vegetation (1970); and, grassland (2000).

5.3.3 Population Density Histogram Analysis

After reviewing the results of the rose diagrams for population density it was observed that the ranges were nearly identical for the five years analyzed. This finding required the investigation of the distribution of the population density to identify an explanation of the nature of the linearity of the variogram ranges. The statistics of the population density data and their log-transformed values are summarized in Table 5.6. In addition, Figure 5.15 shows the log-transformed histograms for the population density data.

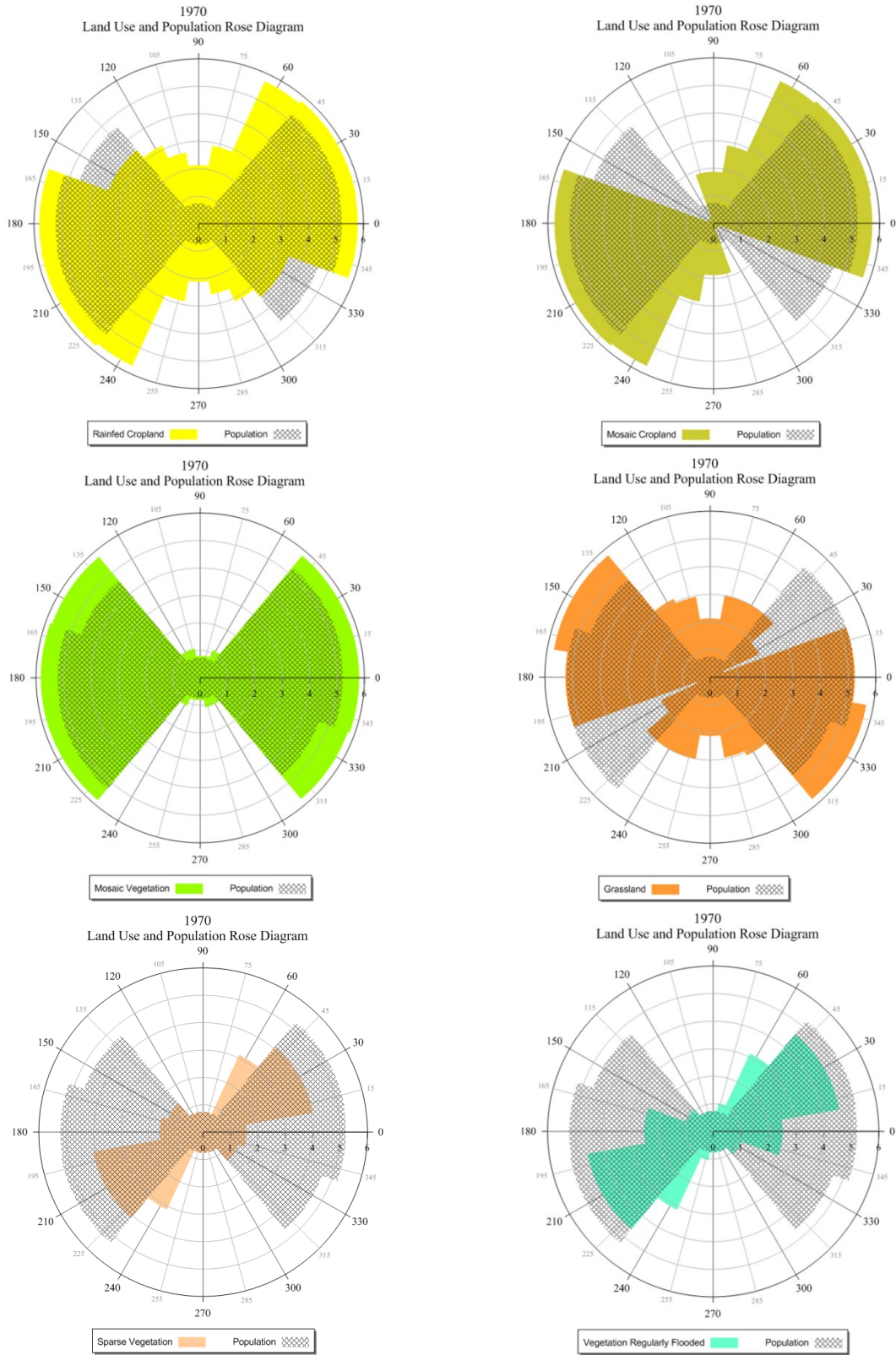


Figure 5.10. 1970 Land Use/Land Cover and Population Density Rose Diagrams.

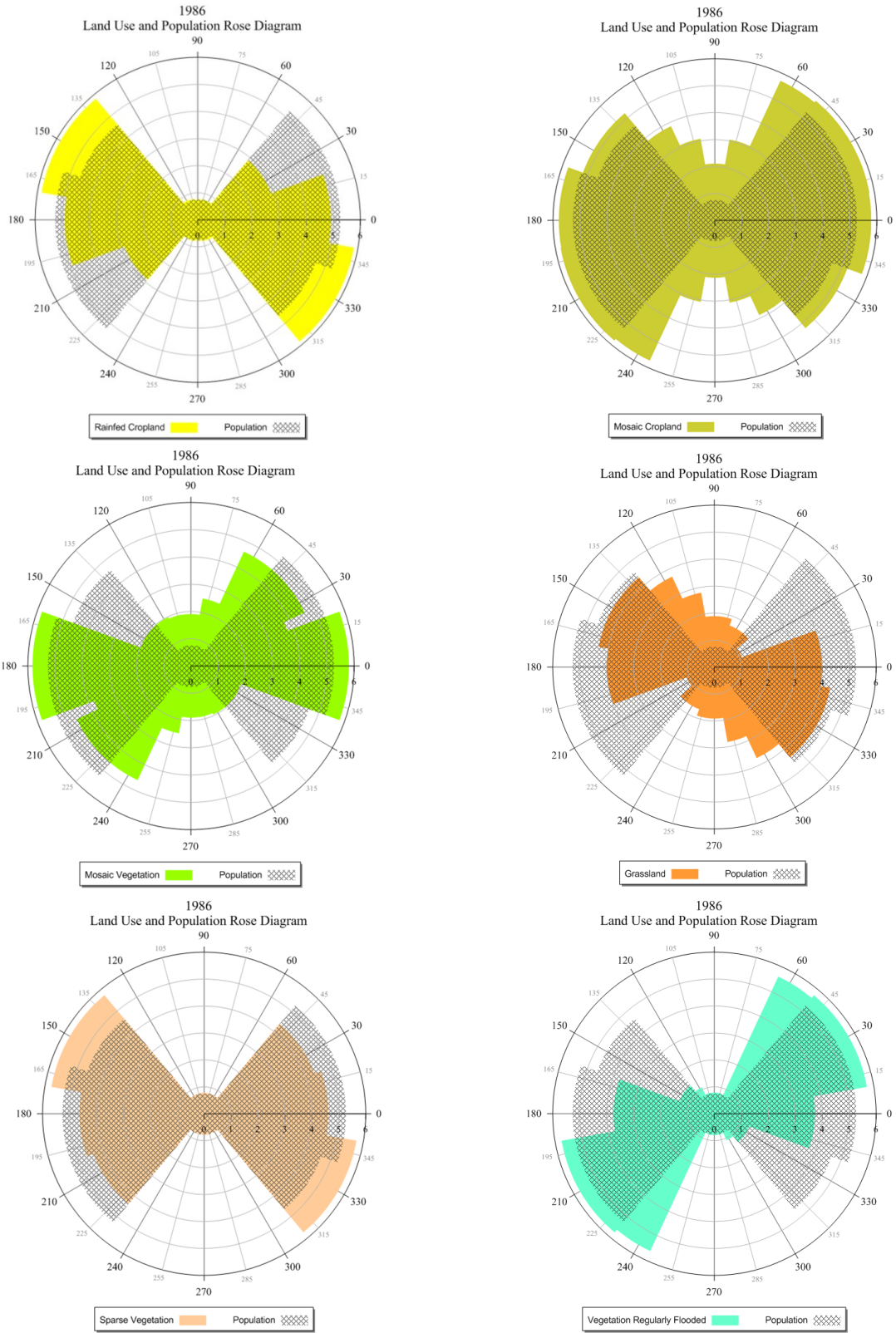


Figure 5.11. 1986 Land Use/Land Cover and Population Density Rose Diagrams.

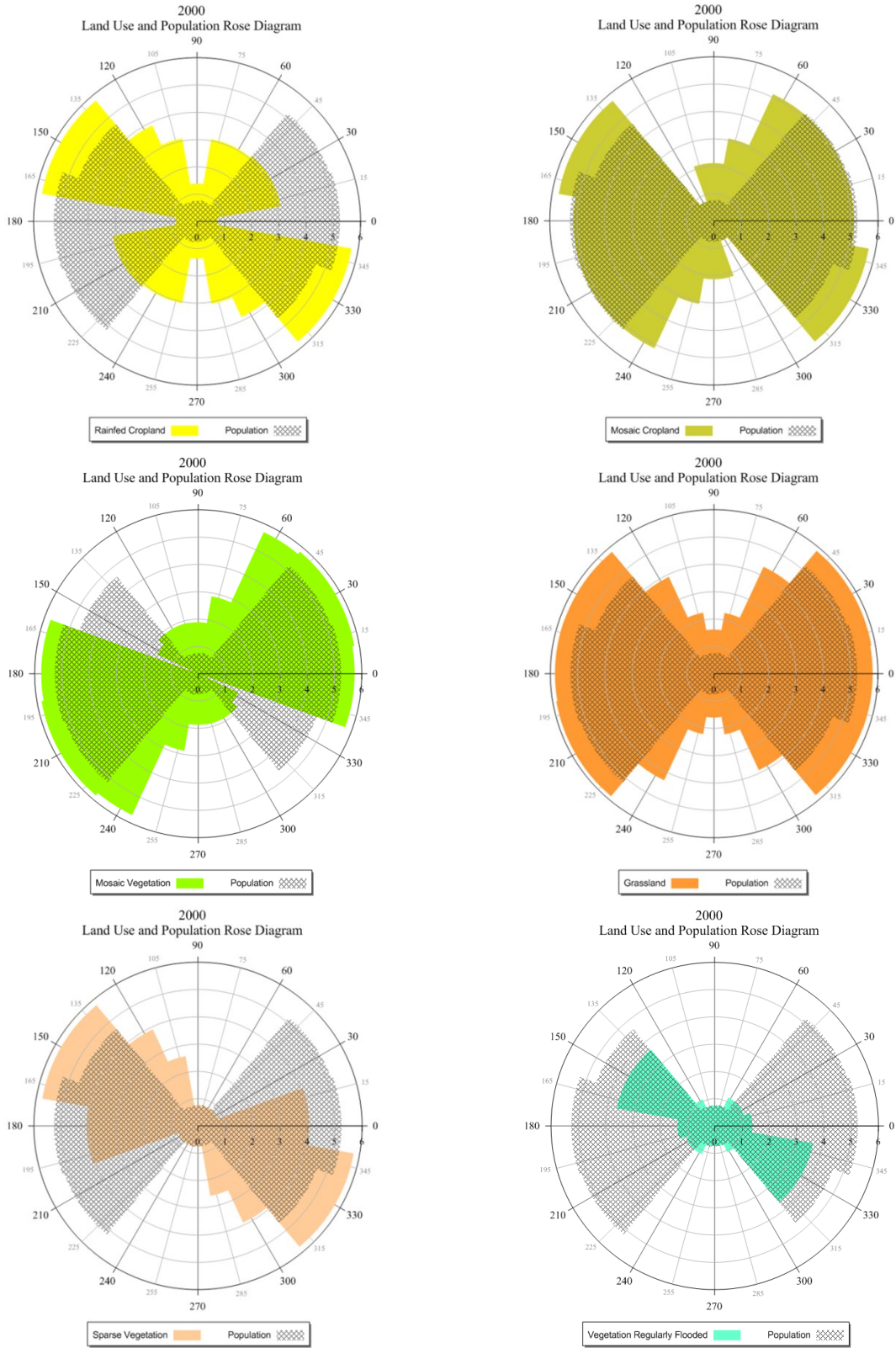


Figure 5.12. 2000 Land Use/Land Cover and Population Density Rose Diagrams.

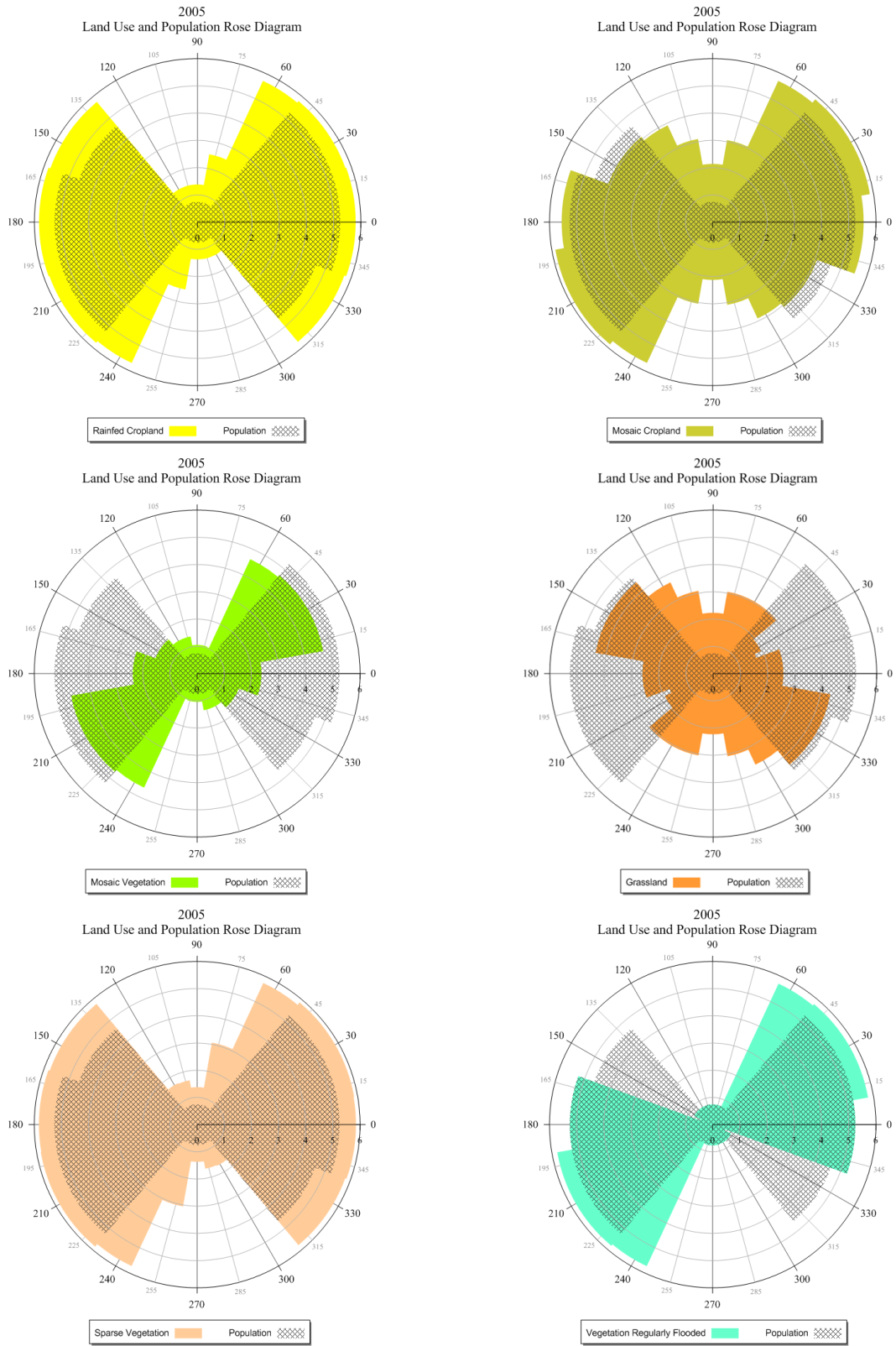


Figure 5.13. 2005 Land Use/Land Cover and Population Density Rose Diagrams.

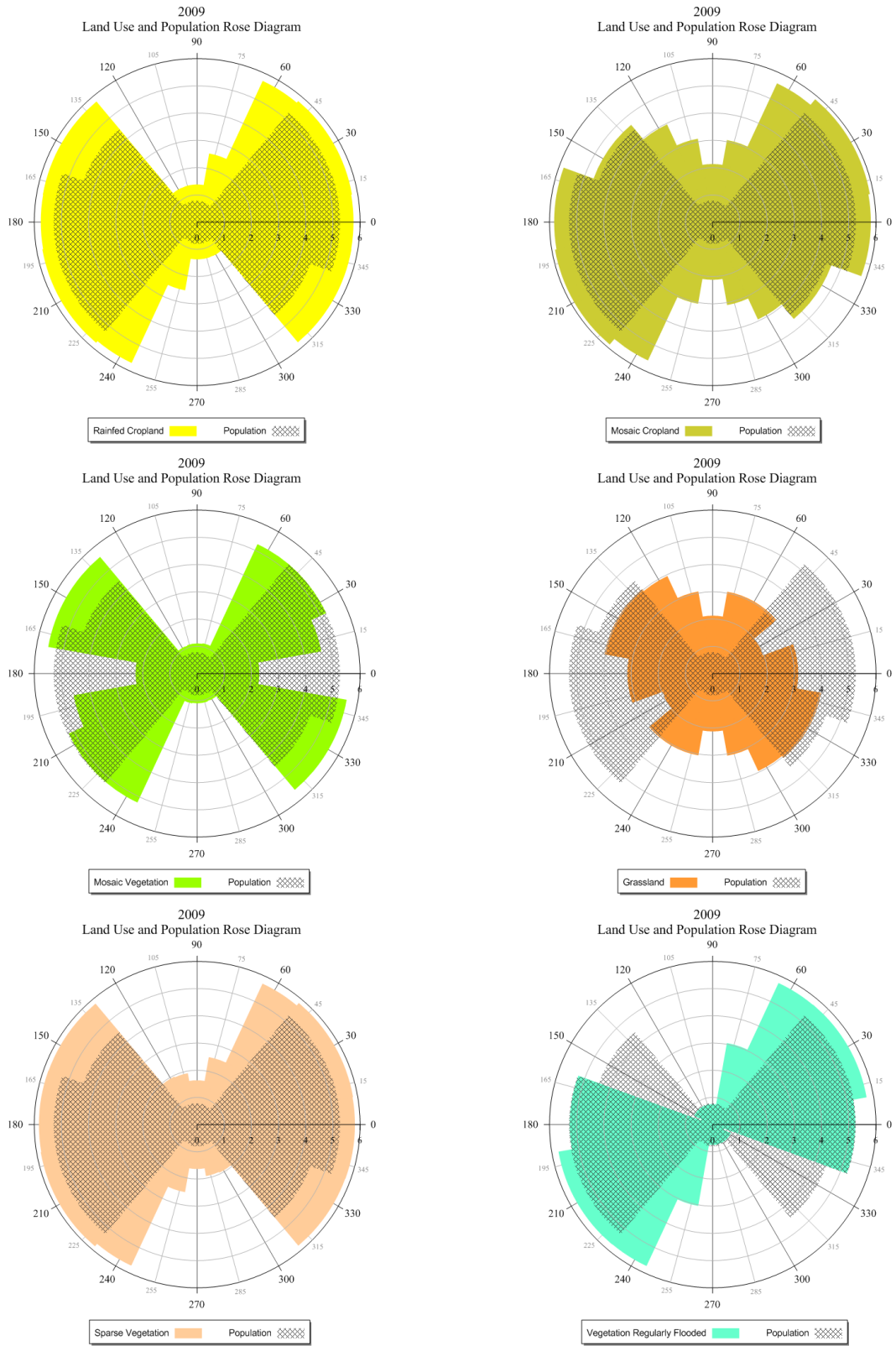


Figure 5.14. 2009 Land Use/Land Cover and Population Density Rose Diagrams.

Table 5.6. Population Density Sample Statistics and Log-Transformed Values.

Statistic	1970	1986	2000	2005	2009
Population Density Samples					
Count	151,863.00	151,863.00	151,863.00	151,863.00	151,863.00
Minimum	0.00	0.00	0.00	0.00	0.00
Maximum	3,442.00	8,727.40	13,906.00	16,093.58	17,843.65
Sum	8,093,439.00	12,459,491.21	18,308,059.00	20,789,565.36	22,774,770.25
Mean	53.29	82.04	120.56	136.90	149.97
Standard Deviation	103.94	233.92	368.59	417.09	457.39
Log-Transformed Population Density Samples					
Count	151,863.00	151,863.00	151,863.00	151,863.00	151,863.00
Minimum	0.00	0.00	0.00	0.00	0.00
Maximum	3.54	3.94	4.14	4.21	4.25
Sum	217,163.14	241,043.40	264,919.96	282,608.29	289,816.69
Mean	1.43	1.59	1.74	1.86	1.91
Standard Deviation	0.53	0.55	0.56	0.47	0.46
Log-Transformed Values Reverted to Original Scale					
Mean	26.91	38.66	55.52	72.60	80.99
Standard Deviation	3.43	3.58	3.67	2.96	2.89

After transforming the population density values to logarithmic scale, it is clear that the standard deviation values are fairly close, which is an indication that the degree of variation between time periods is nearly linear. The population density histograms also show a distribution that is close to the normal distribution, which explains the similarity in range values calculated from the variogram function.

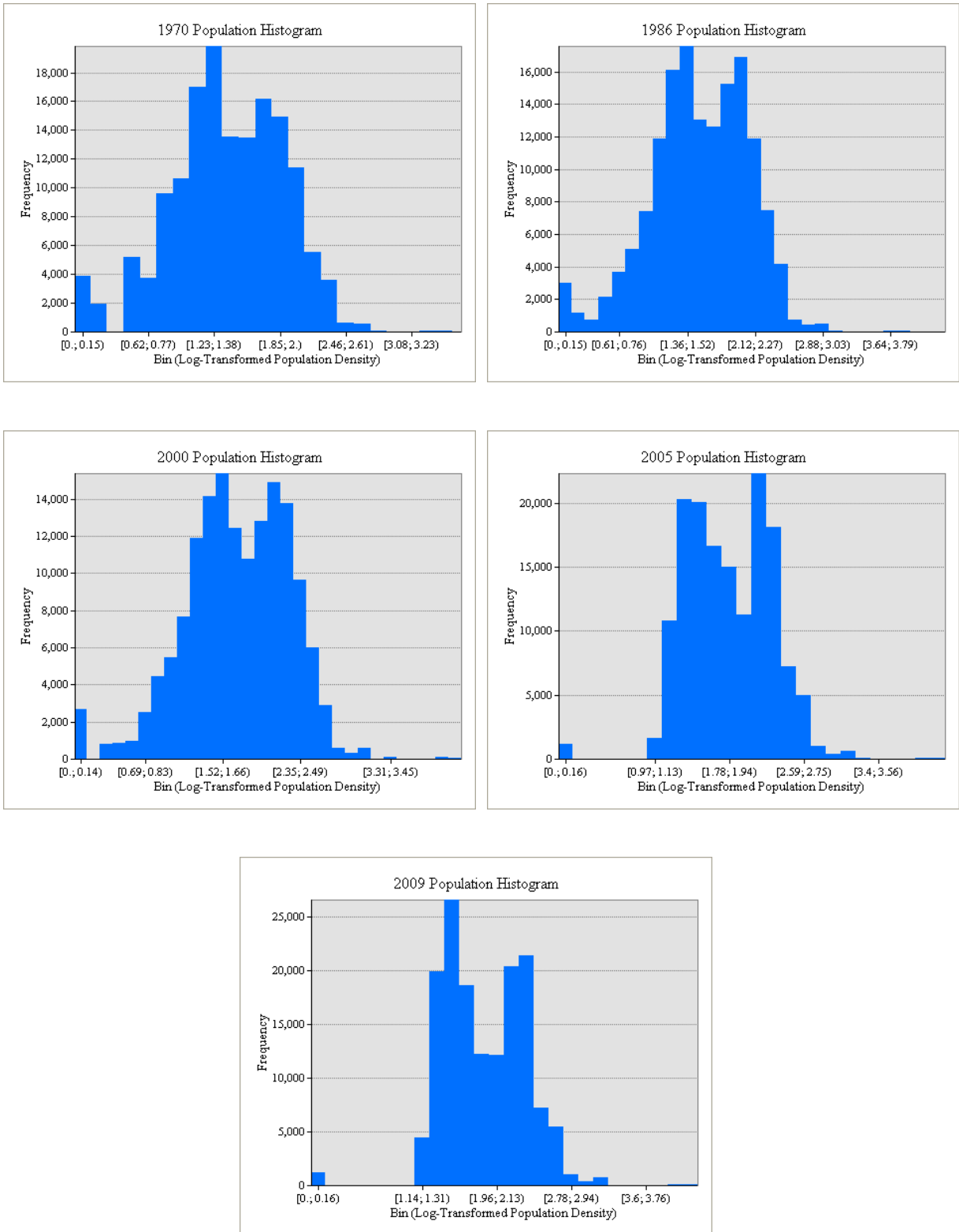


Figure 5.15. Log-Transformed Population Density Histograms.

CHAPTER 6

CONCLUSION

The time-series summary and kriging interpolation of yearly precipitation data helped in the identification of the year 1980 as a time period of significance for the present study. This result supports existing literature documenting the reduction of precipitation in the Sahel during the last five decades. Additional data gathering of historical precipitation and a thorough geostatistical analysis of precipitation variability and its relation to land use/land cover changes may unveil significant results regarding the water budget of Lake Chad.

The calculation of net changes in land use/land cover in the study area indicate significant variations in rainfed cropland, mosaic cropland, mosaic vegetation, grassland, sparse vegetation, and vegetation regularly flooded, between the years of observation: 1970, 1986, 2000, 2005, and 2009. Based on these findings, these six land use/land cover classes were selected for further analysis using the variogram function and rose diagram techniques.

The spatial autocorrelation tool was used to analyze the land use/land cover data and it helped demonstrate that the distribution of the land use/land cover classes is clustered. There is less than 1% likelihood that this pattern results from random chance, which implies a certain degree of autocorrelation in the spatial distribution of the land use/land cover classes. Although land use/land cover distribution shows spatial clustering, the manner in which landscapes in the Sahel transition from forest, wetland, or natural environment into urban or bareland areas requires further analysis.

A new geostatistical tool (Overlapping Neighborhood Statistics) was designed to calculate the overlapping neighborhood statistics with Pearson's correlation coefficient between the land use/land cover and population density raster images. Maps of correlation

coefficient results show areas of direct correlation in red, inverse correlation in blue, and no relation in pale yellow. The 10x10 neighborhood cell unit showed the most clear direct and inverse correlation coefficient results in the study area. The results showed strong direct correlation between population and land use/land cover at urban cores, and strong inverse correlation between the same variables at the southern fringes of the study area.

Indicator variograms of land use/land cover and population density were analyzed in eight coordinate directions (0°, 30°, 45°, 60°, 90°, 120°, 135°, and 150°) with an angular tolerance of 20°, for the five years of observation. The ranges obtained were used to build rose diagrams to identify the land use/land cover classes and directions most closely related to those observed for population density. The classes that most closely match the population density rose diagrams are: mosaic cropland (all years, except 1970); rainfed cropland (1970, 2005, and 2009); sparse vegetation (1986, 2005 and 2009); mosaic vegetation (1970); and, grassland (2000). The shaded areas in Figure 6.1 indicate the years and the classes for which population density and land use/land cover had similar rose diagrams.

	1970	1986	2000	2005	2009
Rainfed Cropland	Shaded			Shaded	Shaded
Mosaic Cropland		Shaded	Shaded	Shaded	Shaded
Mosaic Vegetation	Shaded				
Grassland			Shaded		
Sparse Vegetation		Shaded		Shaded	Shaded
Vegetation Regularly Flooded					

Figure 6.1. Similar Rose Diagrams between Land Use/Land Cover and Population Density.

These results indicate that land use/land cover classes associated with agriculture have a strong connection to the spatial distribution of population density. The years 1986 and 2000 showed dissimilarity in rose diagrams between population density and rainfed cropland, possibly due to the reduction in water-demanding crops during and after the drought of the 1980s. The year 2000 marks a transition period from the drought to a recovery state for the study area. This year shows a correlation between the expansion of grassland and population density, possibly associated with the reemergence pastures for livestock and cattle ranching. After the year 2000, the cropland and sparse vegetation land use/land cover classes show correlation with population density; however, further analysis is required in order to determine whether this is a persistent trend. Vegetation regularly flooded showed no correlation to population density throughout the study, which indicates that this land use/land cover class is influenced by multiple factors that require independent analysis.

Population density histograms for the five years of observation show a nearly normal distribution, which results in similar range and direction values for all population density datasets. This implies that isotropic changes in population density do not affect the range of the variogram function. Furthermore, if the changes are anisotropic, but also linear in time, the ranges of the variogram function are also expected to be similar. This indicates that the variogram function as a spatial comparison tool between population density and land use/land cover change is useful to inspect a single period of observation, but the analysis of trends over time may require a different methodology.

REFERENCES

1. Anderson, J.R., Hardy, E.E., Roach, J.T. and Witmer, R.E. "A land use and land cover classification system for use with remote sensor data." *U.S. Geological Survey Professional Paper No. 964*, 1976: USGS, Washington, D.C.
2. Aymatth2. "Sketch map of the catchment area of the Yobe river in north-east Nigeria." 2009. http://en.wikipedia.org/wiki/File:Yobe_river_catchment_area.png (accessed July 2011).
3. Birkett, C.M. "Synergistic Remote Sensing of Lake Chad: Variability of Basin Inundation." *Remote Sensing of Environment* 72, 2000: 2:218-236.
4. Brown, D.G., Goovaerts, P., Burnicki, A., Li, M.Y. "Stochastic Simulation of Land-cover Change Using Geostatistics and Generalized Additive Models." *Photogrammetric Engineering and Remote Sensing*, 2002: 68(10):1051-1061.
5. Cappelaere, B., et al. "The AMMA-CATCH experiment in the Sahelian area of southwest Niger - Investigating water cycle response to a fluctuating climate and changing environment." *Journal of Hydrology*, 2009: 375:34-51.
6. Clark, I. *Practical geostatistics*. London: Applied Science Publishers, 1979.
7. Coe, M.T., and Foley, J.A. "Human and natural impacts on the water resources of the Lake Chad basin." *Journal of Geophysical Research*, 2001: 106:3349-3356.
8. Cressie, N. *Statistics for Spatial Data*, revised edition. New York: Wiley Interscience, 1993.
9. Desconnets J.C., Taupin, J.D., Lebel T., and Leduc C. "Hydrology of the HAPEX-Sahel central Super-Site: surface water drainage and aquifer recharge through the pool systems." *Journal of Hydrology*. 1997: 188-189:155-178.
10. European Space Agency, (ESA). "GlobCover, ESA Earthnet Online." <https://earth.esa.int/web/guest/data-access/> (accessed October 2011).
11. Famine Early Warning System (FEWS), U.S. Agency for International Development, "Lake Chad; untapped potential." FEWS Special Report 97-4. 1997.
12. Food and Agriculture Organization, (FAO). "GeoNetwork." <http://www.fao.org/geonetwork/srv/en/main.home> (accessed October 2011).
13. Grove, A.T. "African river discharge and the lake levels in twentieth century." In *The Limnology, Climatology and Paleoclimatology of the East African Lakes*, edited by Johnson, T.C., Odada, E., 95-100. Newark: Gordon and Breach, 1996.

14. Isiorho, S.A and Njock-Libii J., “Sustainable water resources management practice.” *Global Networks for Environmental Information*, 1996: 11:855–860.
15. Judex, M., Thamm, H.-P, and Menz, G. “Modelling of land-use changes in a west African catchment.” In *ISPRS Mid-term symposium. 2006 Proceedings: From pixels to processes*, edited by G. Kerle, N. and Skidmore, A. Enschede, 2006.
16. Kimmage, K. and Adams, W. M. “Wetland agricultural production and river basin development in the Hadejia-Jama'are valley, Nigeria.” *The Geographical Journal*, 1992: 158:1-12.
17. Koenig, Felix. “A map of Africa: the Sahel highlighted in orange.” 2009. http://en.wikipedia.org/wiki/File:Sahel_Map-Africa_rough.png (accessed July 2011).
18. Leduc, C., Favreau, G., and Shroeter, P. “Long term rise in a Sahelian water-table: the Continental Terminal in South-West Niger.” *Journal of Hydrology*, 2001: 243:43-54.
19. Lee, J., Odor, R., Babamaaji R., and Goni, I.B. “Groundwater responses to the change of land cover, precipitation and surface water around Lake Chad in Nigeria.” Working paper in preparation for submission to *Journal of Hydrology*, Department of Geosciences, University of Missouri-Kansas City, 2012.
20. Loveland, T.R. and Acevedo, W. “Land Cover Change in the Eastern United States.” In *Status and Trends in Eastern United States Land Cover*. U.S. Geological Survey, Center for Earth Observations and Science, Sioux Falls. <http://landcoverrends.usgs.gov/east/regionalSummary.html> (accessed August 2011).
21. Mackenzie, J. “Land-Use/Land Cover Transitions in Delaware, 2002-2007.” Working paper, College of Agriculture and Natural Resources, University of Delaware, Newark, 2009.
22. Meyer, W.B., and Turner, B.L. “Human-Population Growth and Global Land-Use Cover Change.” *Annual Review of Ecology and Systematics*, 1992: 23:39-61.
23. Moran, P. “Notes on Continuous Stochastic Phenomena.” *Biometrika*, 1950: 37(1):17-23.
24. Mubea, K.W., Mundia, C.N., and Kuria, D.N., “The Use of Markov Chain Analysis in Predicting Land Use/Cover Change in Nyeri.” Working paper, Department of Civil Engineering, Kimathi University College of Technology, Nyeri, Kenya, 2011.
25. National Aeronautics and Spatial Administration, (NASA). “Landsat Science.” <http://landsat.gsfc.nasa.gov> (accessed July 2011).
26. National Oceanic and Atmospheric Administration, (NOAA). “National Climatic Data Center.” <http://www.ncdc.noaa.gov/oa/ncdc.html> (accessed March 2011).

27. Olivry, J.C., Chouret, A., Vuillaume, G., Lemoalle, J., and Bricquet, J. "Hydrologie du Lac Tchad." French Institute of Scientific Research for Cooperative Development (ORSTOM), Monogr. Hydrol., Vol 12, Paris, 1996.
28. Ouedraogo, I. "Land Use Dynamics and Demographic Change in Southern Burkina Faso." PhD diss., Swedish University of Agricultural Sciences, Alnarp, 2010.
29. Roche, M. A. "Traçage hydro-chimique naturel du mouvement des eaux dans le Lac Tchad." Paper presented at the Hydrology of Lakes Symposium, IAHS-AISH 109:18-27, Helsinki, 1973.
30. Seguis, L., et al. "Simulated impacts of climate change and land-clearing on runoff from a small Sahelian catchment." *Hydrological Processes*, 2004: 18:3401-3413.
31. Socioeconomic Data and Applications Center, (SEDAC). "Data Sets." <http://sedac.ciesin.org> (accessed December 2011).
32. Stehman, S.V., and Wickham, J.D. "Assessing Accuracy of Net Change Derived from Land Cover Maps." *Photogrammetric Engineering Remote Sensing* 72, 2006: 2:175-185.
33. Taylor, C.M., Lambin, E.F., Stephenne, N., Harding, R.J., and Essery, R.L.H. "The influence of land use change on climate in the Sahel." *Journal of Climate*, 2002: 15:3615-3629.
34. Tayyebi, A., Delavar, M.R., Saeedi, S., Amini, J. and Alinia, H. "Monitoring land use change by multi-temporal LANDSAT remote sensing imagery." In *Proceedings of the International Society for Photogrammetry and Remote Sensing, Commission VII*, Beijing, 2008.
35. Thompson, J.R. and Polet, G. "Hydrology and land use in a Sahelian floodplain wetland." *Wetlands*, 2000: 20(4):639-659.
36. Tobler, W. "A computer movie simulating urban growth in the Detroit region." *Economic Geography*, 1970: 46(2):234-240.
37. United Nations Environment Programme, (UNEP). "Global Resource Information Database." <http://www.grid.unep.ch> (Accessed December 2011).
38. United States Geological Survey, (USGS). "Global Visualization Viewer." <http://glovis.usgs.gov> (accessed November 2010).
39. Vuillaume, G., "Bilan hydrologique mensuel et modélisation sommaire du régime hydrologique du Lac Chad." French Institute of Scientific Research for Cooperative Development (ORSTOM), Sér. Hydrol., Vol 18(1), 23-72, Paris, 1981.

VITA

Ingrid Milena Tobar was born on July 12, 1982 in Bogota, Colombia. In 2008, she earned a Bachelor of Science Degree in Environmental Studies at the University of Missouri, Kansas City. Subsequently, Ms. Tobar enrolled in the graduate school at the same institution to complete a Master's Degree in Environmental and Urban Geosciences. Ms. Tobar currently works as Environmental Scientist/GIS Analyst for a consulting firm. She may be reached at ingtob@gmail.com.